Translational Oncology 19 (2022) 101389

Contents lists available at ScienceDirect

Translational Oncology

journal homepage: www.elsevier.com/locate/tranon

Original Research

Identification of metastasis-associated exoDEPs in colorectal cancer using label-free proteomics

Xinlu Liu [a], Na Li [b], Chi Zhang [a], Xiaoyu Wu [c], Shoujia Zhang [a], Gang Dong [d], Ge Liu [a,*]

[a] 1st Department of general surgery, The First Affiliated Hospital of Dalian Medical University, No. 193 Union Road, Dalian City, Liaoning Province, China
[b] Department of Gastroenterology, The First Affiliated Hospital of Dalian Medical University, No. 222 Zhongshan Road, Dalian City, Liaoning Province, China
[c] Operating Room, The First Affiliated Hospital of Dalian Medical University, No. 193 Union Road, Dalian City, Liaoning Province, China
[d] Anorectal surgery, Central Hospital of Jinzhou City, No. 51, Section 2, Shanghai Road, Guta District, Jinzhou City, Liaoning Province, China

ARTICLE INFO

Keywords:
Exosomes
Label-free proteomics
Tumor microenvironment (TME)
Metastasis
Colorectal cancer

ABSTRACT

Exosomes are secreted nanovesicles consisting of biochemical molecules, including proteins, RNAs, lipids, and metabolites that play a prominent role in tumor progression. In this study, we performed a label-free proteomic analysis of exosomes from a pair of homologous human colorectal cancer cell line with different metastatic abilities. A total of 115 exoDEPs were identified, with 31 proteins upregulated and 84 proteins downregulated in SW620 exosome. We also detected 30 proteins expressed only in SW620 exosomes and 60 proteins expressed only in SW480 exosomes. Bioinformatics analysis enriched the components and pathways associated with the extracellular matrix, cytoskeleton-related pathways, and immune system changes of colorectal cancer (CRC). Cellular function experiments confirmed the role of SW620 exosomes in promoting the proliferation, migration, and invasion of SW480 cells. Further verifications were performed on six upregulated exoDEPs (FGFBP1, SIPA1, THBS1, TGFBI, COL6A1, and RPL10), three downregulated exoDEPs (SLC2A3, MYO1D, and RBP1), and three exoDEPs (SMOC2, GLG1, and CEMIP) expressed only in SW620 by WB and IHC. This study provides a complete and novel basis for exploring new drug targets to inhibit the invasion and metastasis of CRC.

Introduction

Colorectal cancer (CRC) is the third most common tumor and the second leading cause of cancer-related mortality worldwide [1]. Although modern research has shed light on the pathogenesis of CRC and provides enhanced screening strategies, the prevalence of CRC is still increasing. Despite an improved outcome with the current treatment regimen, a huge number of patients relapse, have distant metastasis, and develop drug-resistant disease within 5 years after operation [2,3]. More than 50% of CRC patients have distant metastasis, particularly in the liver, lungs, and bone. Patients with distant metastasis, notably liver metastasis, have a 5-year survival rate below 50%; however, patients without metastasis can largely be cured by resection of the primary tumor and have a 5-year survival rate exceeding 80%. Therefore, it is very important to clarify the mechanism of CRC invasion and metastasis and identify the key regulating proteins as new biomarkers or therapeutic targets for improving the prognosis of CRC patients.

The tumor microenvironment (TME) has been identified as a resident of a variety of cells, including tumor cells, stromal cells, extracellular matrix (ECM), immune cells, blood vessels, and differentiated cells [4]. It establishes a communication network for crosstalk and signaling between tumor cells, stroma, and other interstitial cells. It is vital for the initiation of tumor proliferation and angiogenesis, evasion of apoptosis and immune surveillance, suppression of the immune system, and metastasis. The intercellular communication of the TME creates a niche for reprogramming resident cells, extracellular matrix, and angiogenesis, which prompts the metastasis of cancer cells.

Exosomes are vital cell-cell communicators of information within the TME by horizontal transfer of proteins, lipids, DNA, and RNA [5]. It is a small vesicle with a diameter of 30–150 nm released from the majority of cell types and has a typical lipid bilayer structure [6]. Exosomes exist in cell culture supernatants, serum, plasma, saliva, urine, amniotic fluid, and other biological fluids. Tumor-derived exosomes modulate stromal cells, reprogram ECM, induce transformation of normal cells adjacent to the tumor, stimulate endothelial cells to form vascular, and alter the invasive behavior of tumor cells. Exosomes play an important role in regulating tumor metastasis, especially liver metastasis, through various functions. For example, exosomes from the TME of CRC can reprogram

* Corresponding author.
E-mail address: liuge0802@163.com (G. Liu).

https://doi.org/10.1016/j.tranon.2022.101389
Received 3 September 2021; Received in revised form 20 December 2021; Accepted 28 February 2022

the cancer cell metabolic machinery to increase glycolysis by inhibiting mitochondrial oxidative phosphorylation and contribute toward immune-induced tumor dormancy and antitumor immunotherapy. Identifying the key regulatory exosomal proteins related to metastasis and elucidating their functions are very important for exploring new therapeutic targets for inhibiting CRC metastasis.

Proteomics is considered valuable for early disease diagnosis, prognosis, and monitoring of disease development. Label-free, or unlabeled quantitative technology, is the mass spectrometry analysis of protein enzymatic peptides by liquid chromatography-mass spectrometry (LC-MS) [7]. It overcomes the limitations of traditional isotope labeling, which necessitates a high sample concentration. It is not limited by the labeling kit and can be used for mass sample detection. Moreover, it has less pre-processing, more original information of samples, and a higher coverage for low-abundance peptides to determine the most precise information.

SW620 (highly metastatic) and SW480 (weakly metastatic) are a pair of homologous human CRC cell line with different metastatic abilities. In this study, we first performed the cellular function experiments and confirmed the promoting role of SW620 exosomes on the proliferation, migration, and invasion of SW480 cells. We then used a label-free differential proteomics on this pair of cell lines to identify the exosomal differentially expressed proteins (exoDEPs) regulating CRC metastasis in the TME. After analysis, 115 exoDEPs (31 upregulated and 84 downregulated in SW620 exosomes), and 90 “all or no” exoDEPs (30 only in SW620 and 60 only in SW480) were identified. Bioinformatics analysis enriched the components and pathways associated with the ECM, cytoskeleton-related pathways, and immune system changes of CRC. Further validation results of the 12 selected exoDEPs were consistent with the proteomics results. The exoDEPs identified in this study provide new potential therapeutic targets and research directions in the TME for CRC metastasis.

Materials & methods

Ethics

This study was approved by the Institutional Review Board of the First Affiliated Hospital of Dalian Medical University. Written informed consent was obtained from all patients.

Cell culture

CRC cell lines SW620 (highly metastatic) and SW480 (weakly metastatic) were purchased from the Chinese Academy of Sciences cell bank. All cell lines were incubated in DMEM (Gibco, Thermo Fisher Scientific, Waltham, MA, USA) supplemented with 10% fetal bovine serum (FBS; Gibco, Thermo Fisher Scientific), 100 U/mL penicillin G, and 100 μg/mL streptomycin (Gibco, Thermo Fisher Scientific) at 37 °C and 5% CO_2/95% air.

Exosome extraction

SW480 and SW620 cells were cultured in complete growth medium. After the cells were cultured to nearly 70% confluence, the medium was replaced with exosome-free medium, and the cells were incubated for an additional 48 h. The primary supernatants were collected and centrifuged at 4 °C for 30 min at 2×10^3 g to remove dead cells for purification (three biological replicates). Next, we isolated the extracellular vesicles (EVs) by ultracentrifugation. In brief, the purified supernatants were placed in ultra-high-speed centrifuge tubes (balanced with 1×PBS) and centrifuged at 110×10^3 g for 75 min at 4 °C. We then obtained the exosome pellets and resuspended it in 1 × PBS. The EVs suspension was added to the purification column and centrifuged at 4 °C for 5 min at 4×10^3 g, and the effluent was the purified exosomes. An electron micrograph and nanoparticle tracking analysis (NTA) of purified exosomes were subsequently performed.

Protein extraction and determination of protein concentration

A 200 μL SDT lysate (4% SDS, 100 mM Dithiothreitol (DTT), and 100 mM Tris HCl) was added to each purified exosome sample. The exosomes were broken by ultrasound for 2 min, soaked in boiling water for 5 min, and centrifuged at 20×10^3 g at 4 °C for 20 min. The supernatant was collected, and the protein was quantified using the BCA method. The FASP method was used for the enzymolysis. The steps were as follows: an appropriate amount of DTT was added to each sample until its final concentration was 100 mm, boiling water bath for 5 min, and cooling to room temperature, 200 μL UA buffer (8 m urea, 150 mm Tris HCl, pH 8.0) was added and mixed well. The sample was transferred to a 10 kDa ultrafiltration centrifuge tube and centrifuged at 12×10^3 g for 15 min, 200 μL UA buffer was added and centrifuged 12×10^3 g for 15 min and the filtrate was discarded. A solution of 100 uL IAA (50 mM IAA in UA) was added, oscillated at 600 rpm for 1 min, kept away from light for 30 min, and centrifuged at 12×10^3 g for 10 min. A solution of 100 uL UA buffers added, centrifuged 12×10^3 g for 10-min and repeated twice. A solution of 100 uL NH_4HCO_3 buffer was added and centrifuged for 14×10^3 g, and this step was repeated twice for 10 min. A solution of 40 uL trypsin buffer (6 μg trypsin in 40 uL NH_4HCO_3 buffer) was added, centrifuged at 600 rpm for 1 min, and stored in 37 °C for 16–18 h. After centrifugation at 12×10^3 g for 10 min, the filtrate was collected, and 0.1% Trifluoroacetyl (TFA) solution was added. The peptides were desalted using a C18 cartridge and freeze-dried under vacuum. The peptides were dried and dissolved in 0.1% FA. The peptide concentration was determined using LC-MS analysis.

LC-MS/MS analysis

An appropriate amount of the peptide was taken from each sample and separated using an easy NLC 1200 chromatography system (Thermo Fisher Scientific, Waltham, MA, USA). Buffer solution: 0.1% formic acid solution; B solution: 0.1% formic acid acetonitrile solution (acetonitrile: 85%). The column was equilibrated to 95%. The sample was injected into a trap column (100 μm × 20 mm, 5 um, C18, Dr. Maisch GmbH) and then separated on a chromatographic column (75 μm × 150 mm, 3 um, C18, Dr. Maisch GmbH) at the flow rate of 300 NL/min. The liquid gradient was set as follows: 0–2 min, with a linear gradient of liquid B as 5%–8%; 2–90 min, with a linear gradient of liquid B as 8%–23%; 100 min, with a linear gradient of liquid B as 23%–40%; 100–108 min, with a linear gradient of liquid B as 40%–100%; and 120 min, with a linear gradient of liquid B as 100%. The peptides were separated and analyzed by data-dependent acquisition mass spectrometry with a Q-active plus mass spectrometer (Thermo Fisher Scientific, Waltham, MA, USA). The analysis time was 120 min; detection mode, positive ion; scanning range of parent ion, 300–1800 m/Z; resolution of primary mass spectrometry, 70×10^3 m/Z200; AGC target, 1E6; and primary maximum it, 50 ms. Peptide secondary mass spectrometry analysis was performed according to the following methods: MS2 scan was triggered after each full scan; resolution, 17,500 at m/z 200; AGC target, 1E5; maximum, 50 ms; MS2 activation type, HCD; isolation window, 1.6th; and normalized collision energy, 27.

Protein identification, quantification, and bioinformatic analyses

The mass spectrometry database retrieval software used in this project is maxquant1.6.0.16. The protein database is from the UniProt protein database (download: 08/05/2019; Homo sapiens: 173,282 entries). Maxquant library search software analysis parameter settings were as follows: Enzyme: Trypsin; Max Missed Cleavages: 2; Main search Peptide Tolerance: 4.5 ppm; First search Peptide Tolerance: 20 ppm; First search Peptide Tolerance: 20 ppm; Fixed modifications: Carbamidomethyl (C); Variable modifications: Oxidation(M), Acetyl (Protein N-

term); PSM (Peptide-Spectral Matching) FDR: 0.01; Protein FDR: 0.01; Protein quantification: Razor and unique peptides were used; LFQ: True; LFQ min. ratio count: 1; Match between runs: True.

After analyzing, all exosomal proteins were reliably identified and quantified based on P-value,0.05. Protein ratios with 2.0-fold change was considered to be differentially expressed. The proteins identified obviously more than 2.0-fold change between this pair of cell lines were identified as "all or no" proteins. For cell components, biological processes and molecular functions were identified using R software (version 3.6.3) for gene ontology (GO) annotation. Pathway analysis and enrichment of exoDEPs were annotated using the Kyoto Encyclopedia of Genes and Genomes (KEGG) database (http://www.genome.jp/kegg/pathway) using R software (version 3.6.3). For GO and KEGG analysis, seven R software packages, namely, "colorspace," "stringi," "ggplot2," "DOSE," "clusterProfiler", "org.Hs.eg.db"and "enrichplot," were used to analyze and to generate the figures. Interaction between exoDEPs was analyzed using Cytoscape (version 3.8.2) [8]. The enrichment analysis was determined by a two-tailed Fisher's exact test to identify the enrichment of the differentially expressed proteins against the background of all identified proteins with a corrected P-value,0.05.

Western blot

Western blotting was performed as described previously [9]. Primary antibodies against CD9, CD63, CD81, HSP90, FGFBP1, SIPA1, THBS1, TGFBI, COL6A1, RPL10, SLC2A3 (GLUT3), MYO1D, RBP1, SMOC2, GLG1, and CEMIP (Protein-Tech Group, Rosemont, IL, USA) were used.

Western blotting was performed to verify the expression of exosome marker proteins and selected exoDEPs in SW620 and SW480 exosomes. Equivalent amounts of total protein (20 μg) were resolved by 10% sodium dodecyl sulfate polyacrylamide gel electrophoresis, and the antibodies were diluted as follows: anti-CD9 (1:1000), anti-CD63 (1:1000), anti-CD81 (1:2000), anti-HSP90 (1:200), anti-FGFBP1 (1:500), anti-SIPA1 (1:2000), anti-THBS1 (1:500), anti-TGFBI (1:200), anti-COL6A1 (1:200), anti-RPL10 (1:1000), anti-GLUT3 (1:500), anti-MYO1D (1:200), anti-RBP1 (1:500), anti-SMOC2 (1:500), anti-GLG1 (1:1000), and anti-CEMIP (1:1000) (Protein-Tech Group, Rosemont, IL, USA). Proteins were detected using an enhanced chemiluminescence reagent (Santa Cruz Biotechnology, Dallas, TX, USA). Western blot signals were quantified using FluorChem E (Protein Simple, San Jose, CA, USA). All analyses were performed using western blots in at least two biological replicates.

Clinical sample collection and IHC

To identify the exoDEPs in clinical human CRC pathologic tissues, 33 CRC samples from 11 patients were retrospectively selected from the pathology database of the Affiliated First Hospital Dalian Medical University, China, between 2020 and 2021, for IHC analysis. All patients received routine preoperative preparation and surgical therapy. None of the patients had a family history of cancer nor received preoperative neoadjuvant therapy. There were five cases (45.45%) combined with clinical and pathological diagnosed regional lymph node metastasis (stage III/IV), and six cases (54.54%) without (Stage I/II). This retrospective study was approved by the First Affiliated Hospital of Dalian Medical University Medical Research and Ethics Committee. Written informed consent was obtained from all patients prior to tissue acquisitions. The clinical stage of the patients was defined according to the American Joint Committee on Cancer TNM staging system. Detailed patient clinical information is shown in Table 5.

The paraffin-embedded tissue sections were deparaffinized, dehydrated through graded alcohols, and subjected to antigen retrieval using citrate buffer (pH 6.0) for 7 min at high heat. The sections were washed with PBS and blocked with 0.3% hydrogen peroxide. The slides were incubated at 4 °C overnight with the following primary antibodies: anti-FGFBP1 (1:200), anti-SIPA1 (1:200), anti-THBS1 (1:200), anti-TGFBI (1:200), anti-COL6A1 (1:200), anti-RPL10 (1:200), anti-GLUT3 (1:200), anti-MYO1D (1:200), anti-RBP1 (1:200), anti-SMOC2 (1:200), anti-GLG1 (1:200), and anti-CEMIP (1:200) (Protein-Tech Group, Rosemont, IL, USA). The slides were visualized using a diaminobenzidine chromogen solution (Dako, Glostrup, Denmark) and counterstained with routine hematoxylin, followed by dehydration with graded ethanol series and mounting of the slides. The immunostaining densities of proteins were quantitatively assessed using NIS-Elements BR 3.0 (Nikon, Tokyo, Japan). In brief, after placing the sections on a microscope (Nikon E800), the images were transferred to a computer using a digital camera (Nikon 80i). Three visual fields were randomly inspected on all slides under high-power magnification. The mean optical densities of the positive areas were measured. The results are expressed as the exact values of the relative optical density units.

Cell proliferation assay

Cell proliferation assays were performed using a Cell Counting Kit-8 (CCK-8, KeyGEN BioTECH, Jiangsu, China) according to the manufacturer's protocol. Exosomes equaling 500 ng of exosomal proteins were added per well, if needed.

In vitro migration and invasion assay

Migration and invasion assays using the Transwell system (24 wells, 8 μm pore size filters, Costar, New York, USA) were performed as described in our previous studies [9]. Exosomes equaling 5 μg of exosomal proteins were added to the upper chamber together with the cells, if needed.

Statistical analysis

Statistical analyses and graphics were conducted using GraphPad Prism 9.0 (GraphPad Software, San Diego, CA, USA). Comparisons of quantitative data were made using Student's *t*-test (two-tailed; $P < 0.05$, considered statistically significant). Results are presented as mean ± standard error of the mean.

Results

Isolation and identification of exoDEPs secreted by SW620 and SW480 cell lines

To identify the exosomal proteins closely associated with CRC metastasis, we used a pair of homologous human CRC cell lines, SW620 (highly metastatic) and SW480 (weakly metastatic), as the model system. Under the light microscope, SW620 showed a spherical shape and discrete growth pattern, while SW480 showed a shuttle shape and aggregate growth pattern (Fig. 1A). After isolation, transmission electron microscopy (TEM) was used to visualize the sizes and structures of the prepared exosomes. As indicated in Fig. 1C, exosomes were detected as a heterogeneous population of small (< 150 nm) particles showing round and cup-shaped morphology electron micrographs. NTA confirmed the observed size distributions (Fig. 1D). Median sizes of 116.8 nm (mean 120.3 ± 6.64 nm) and 111.8 nm (mean 112.0 ± 5.60 nm) were observed for SW620-exo and SW480-exo, respectively. Particle concentrations were calculated resulting in 5.4×10^7/mL (mean $5.3 \pm 1.1 \times 10^7$/mL) (SW620-exo) and 8.6×10^7/mL (mean $8.6 \pm 1.7 \times 10^7$/mL) (SW480-exo). Expressions of exosomal markers CD9, CD63, CD81, and HSP90 were verified by WB (Fig. 1B). These vesicles were used for downstream proteomic analyses.

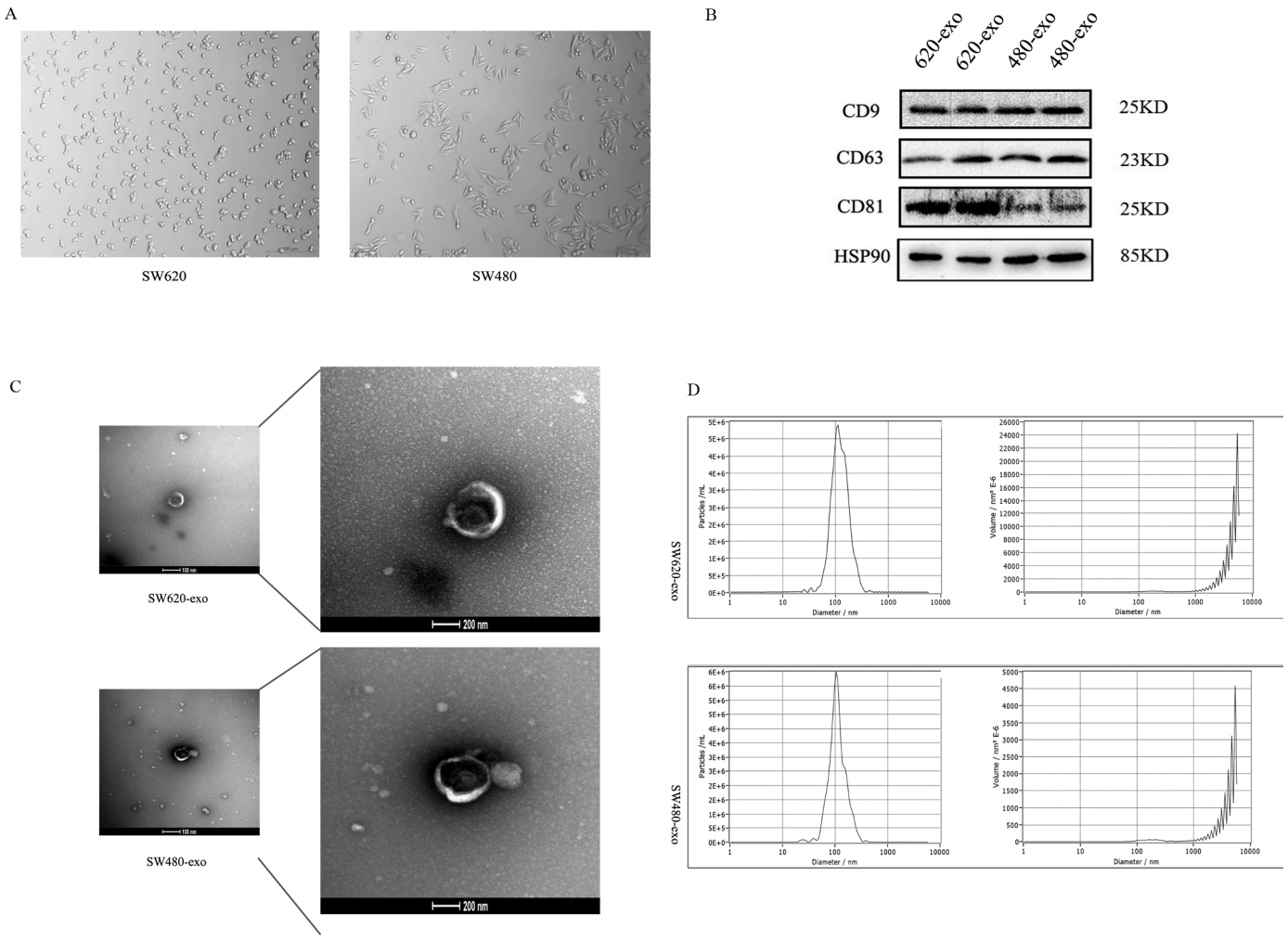

Fig. 1. Identification of exosomes. (A) Cell morphology and distribution characteristics under Light microscope. (B) Western blot analysis confirmed exosome-specific and cell-specific protein marker expression. Protein sizes are indicated. (C) Transmission electron microscopy (TEM) pictures visualized the morphology of isolated exosomes. Scale bar: 100 nm. (D) Nanoparticle tracking analysis (NTA) revealed the size distribution and particle concentration of isolated exosomes.

Label-free proteomics identify the metastasis-associated exoDEPs in the CRC

After purifying the exosomes of SW620 and SW480, we first lysed the exosomes to obtain the proteins and further hydrolyzed the protein peptides, which were directly semi-quantitatively detected by liquid chromatography-mass spectrometry (LC-MS). According to the principle of label-free proteomics, the frequency (counts) of peptide capture and detection in mass spectrometry is positively correlated with its abundance in the mixture. Therefore, the protein count detected by mass spectrometry reflects the abundance of protein. Using an appropriate mathematical formula, the mass spectrometry detection count can be linked with the amount of protein to quantify the secreted proteins of the two cells to determine the upregulated or downregulated proteins with the largest expression difference and the "all or none" expressed proteins. The technical schematic diagram and the heat map and volcano map of the differential proteomics are shown in Fig. 2.

In total, 942 exoDEPs were quantified in all three mechanical and biological repetitions and searched against the database. By setting the quantification ratio 2.0-fold change as the threshold, 115 exoDEPs (2.0-fold change, $P < 0.05$) were identified, including 31 upregulated and 84 downregulated proteins in SW620 exosomes. The top 10 upregulated and downregulated exosomal proteins in SW620 are listed in Tables 1 and 2, respectively. (Table S1 lists all 31 upregulated proteins and Table S2 lists all 84 downregulated proteins in SW620 exosomes).

To find more accurate and in-depth information associated with metastasis of CRC, we also identified 90 "all or none" exoDEPs in this analysis, wherein 30 proteins were found only in SW620 exosomes, and 60 proteins were found only in SW480 exosomes. The top five proteins expressed only in SW620 and SW480 exosomes are listed in Tables 3 and 4, respectively. (Table S3 lists all 30 proteins expressed only in SW620 exosomes, and Table S4 lists all 60 proteins expressed only in SW480 exosomes).

Exosomes from SW620 promoted the proliferation, migration, and invasion of SW480

To investigate the role of exosomes in the proliferation of CRC cell lines, we performed CCK-8 assays. The results showed that after treatment with SW620 exosomes, the proliferation of SW480 cells increased. After treatment with SW480 exosomes, the proliferation of SW620 cells decreased more obviously (Fig. 3A). This result indicated that SW620 exosomes could promote the proliferation of SW480 cells, whereas SW480 exosomes could inhibit the proliferation of SW620 cells, thus showing that the inhibitory role of SW480 exosomes was stronger. To investigate the role of exosomes in the migration and invasion of CRC cell lines, we performed transwell assays. Results showed that after treatment with SW620 exosomes, migration and invasion of SW480 were significantly enhanced by 60% (Fig. 3B-C). These results indicated that exosomes play a crucial role in CRC invasive behaviors through

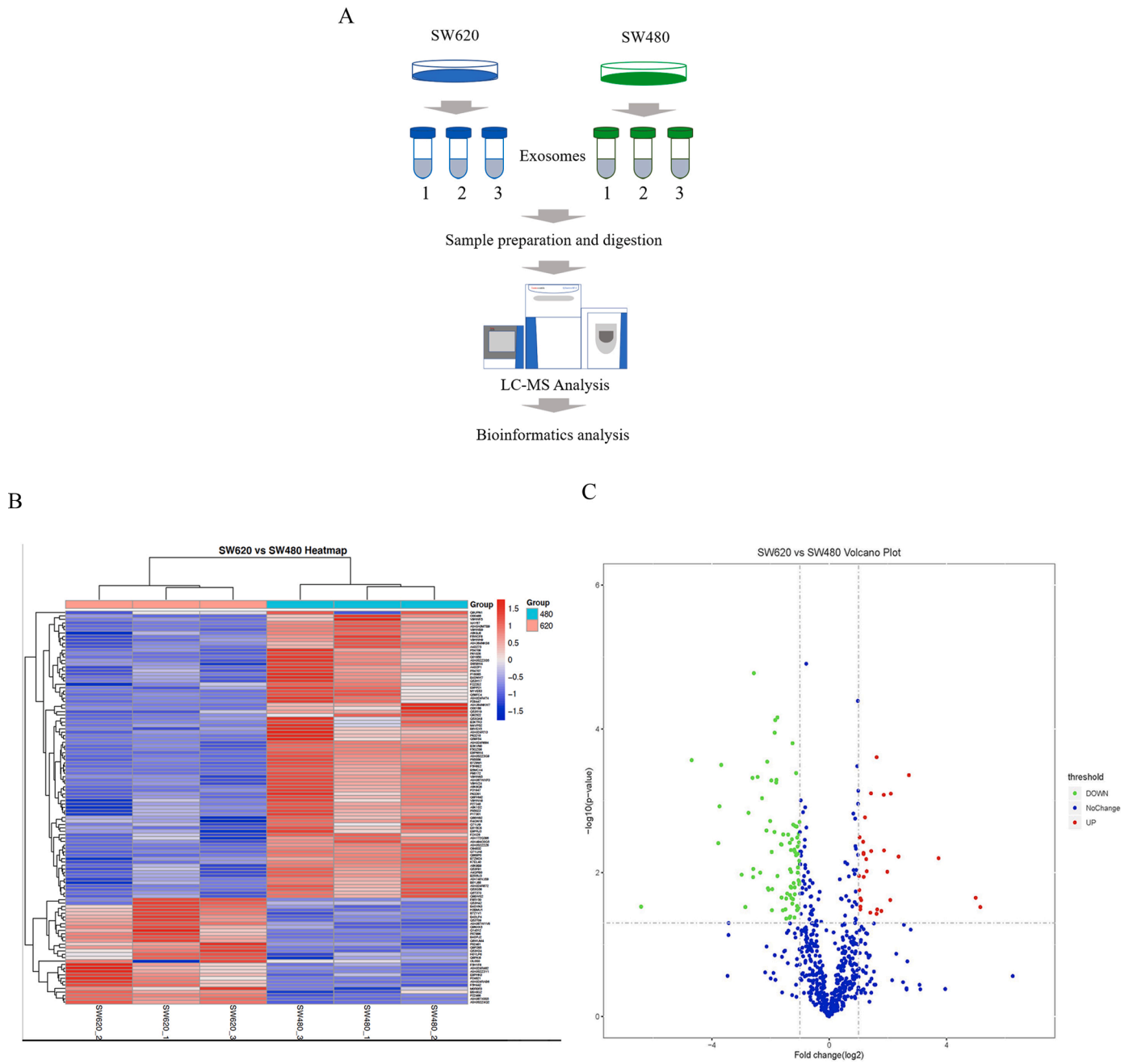

Fig. 2. . Label-free proteomics was used to identify the metastasis-associated exoDEPs in SW620 and SW480 cells. (A) The technical schematic diagram of label-free proteomics. (B) The heat map shows the clustering results of significant differentially expressed proteins and whether there are differentially expressed in SW620 vs. SW480 comparison group. (C) Volcano plot shows non-regulated proteins (blue) and significantly up (red) and downregulated (green) proteins in SW620 exosomes. The X axis represents log2-transformed fold change values. Y axis shows the −log10 p-value adjusted for multiple comparisons.

extracellular effects, and the promoting role of SW620 exosomes on SW480 cells was very prominent. The changes in cell shape and pseudopodia of this pair of cell lines were not obvious after treatment.

In summary, the promoting role of the exosomal proteins of SW620 and the inhibiting role of the exosomal proteins of SW480 on tumor invasion and metastasis have been elucidated in the cellular functional experiments above. However, the key proteins and pathways involved remained unknown. Therefore, we performed bioinformatics analysis for all exoDEPs to explore in-depth information in further research.

Functional enrichment analysis and protein-protein interaction network analysis of upregulated and downregulated exoDEPs

To characterize the functions and subcellular locations of the upregulated and downregulated exoDEPs between this pair of cell lines, GO annotation, KEGG pathway, and PPI network analysis were carried out. The GO annotation analysis included biological processes, cellular components, and molecular functions. For biological process classification, exoDEPs are mainly associated with cell junction assembly, cell junction organization, extracellular structure organization, regulation of cellular component size, and viral life cycle. For cellular components, exoDEPs are mainly associated with cell-substrate adherens junctions, cell-substrate junctions, focal adhesions, melanosomes, and pigment

Table 1
Top 10 upregulated exoDEPs in SW620.

Protein IDs	Protein names	Gene names	Sequence coverage [%]	Mol. weight [kDa]	SW620/ SW480	P. value
Q14512	Fibroblast growth factor-binding protein 1	FGFBP1	19.2	26.264	35.5622503	0.03006523
P24821	Tenascin	TNC	31.2	240.85	31.9171121	0.02235115
Q96FS4	Signal-induced proliferation-associated protein 1	SIPA1	0.7	101.82	13.2653467	0.00628316
Q8N6F7	Galanin peptides	GAL	25.2	13.302	6.59087605	0.00043934
P07996	Thrombospondin-1	THBS1	25.7	129.38	5.15722985	0.00596742
Q15582	Transforming growth factor-beta-induced protein ig-h3	TGFBI	26.4	74.68	4.29955673	0.00079523
Q08380	Galectin-3-binding protein	LGALS3BP	30.4	65.33	4.23649295	0.02398548
P18827	Syndecan-1	SDC1	10.6	16.936	3.95082411	0.00969672
P98160	Basement membrane-specific heparan sulfate proteoglycan core protein	HSPG2	31.7	464.01	3.65451637	0.00490496
P50995	Annexin A11	ANXA11	39.7	45.597	3.63266542	0.00082676

Table 2
Top 10 downregulated exoDEPs in SW620.

Protein IDs	Protein names	Gene names	Sequence coverage [%]	Mol. weight [kDa]	SW620/ SW480	P. value
P11169	Solute carrier family 2, facilitated glucose transporter member 3	SLC2A3	20.8	31.874	0.011749168	0.0296785
O94832	Unconventional myosin-Id	MYO1D	28.2	116.2	0.038787995	0.00027188
P29374	Retinol-binding protein 1	RBP1	56	10.644	0.072787169	0.00388128
P98172	Ephrin-B1	EFNB1	16.2	38.006	0.074930021	0.00119442
P08133	Annexin A6	ANXA6	37.1	75.872	0.078012029	0.00031708
Q96TA1	Niban-like protein 1	C9orf88	10.9	82.682	0.126490412	0.01065253
Q9Y696	Chloride intracellular channel protein 4	CLIC4	26.6	26.694	0.137963444	0.03000887
P05556	Integrin beta-1	ITGB1	20.9	88.414	0.14864844	0.00146909
P16422	Epithelial cell adhesion molecule	EPCAM	34.8	37.893	0.163589346	0.00048008
P61081	NEDD8-conjugating enzyme Ubc12	UBE2M	8.7	20.9	0.165887295	0.0115204

Table 3
Top 10 exoDEPs only expressed in SW620.

protein IDs	Protein names	Gene names	Sequence coverage [%]	Mol. weight [kDa]	Sequence coverage 480-mean [%]	Sequence coverage 620-mean [%]	Intensity	LFQ intensity 480-mean	LFQ intensity 620-mean
Q8NCR9	Clarin-3	CLRN3	12.4	25.321	3.866667	6.6	79,843,000	0	34,011,666.7
Q8NDC0	MAPK-interacting and spindle-stabilizing protein-like	MAPK1IP1L	6.9	24.269	0	4.6	58,364,000	0	30,015,333.3
Q8WUJ3	Cell migration-inducing and hyaluronan-binding protein	CEMIP	11.2	153	0	7.2	5.88E+08	0	283,110,000
Q92896	Golgi apparatus protein 1	GLG1	3.4	134.55	0	2.766667	1.37E+08	0	68,899,333.3
Q9H3U7	SPARC-related modular calcium-binding protein 2	SMOC2	17.7	49.674	0	16.86667	8.83E+08	0	448,096,667

Table 4
Top 10 exoDEPs only expressed in SW480.

Protein IDs	Protein names	Gene names	Sequence coverage [%]	Mol. weight [kDa]	Sequence coverage 480-mean [%]	Sequence coverage 620-mean [%]	Intensity	LFQ intensity 480-mean	LFQ intensity 620-mean
P05121	Plasminogen activator inhibitor 1	SERPINE1	2.5	45.059	1.666666667	0	36,502,000	11,615,333.33	0
P50151	Guanine nucleotide-binding protein G(I)/G(S)/G(O) subunit gamma-10	GNG10	42.6	7.2053	42.6	0	98,311,000	29,713,666.67	0
P41221	Protein Wnt-5a	WNT5A	9	40.886	7	0	213,720,000	62,549,666.67	0
P31146	Coronin-1A	CORO1A	3.9	51.026	1.866666667	0	25,254,000	8,137,000	0
Q92817	Envoplakin	EVPL	0.4	231.63	0.4	0.133333333	22,870,000	6,611,900	0

granules. For molecular function, exoDEPs are mainly associated with actin binding, actin filament binding, cadherin binding, calcium-dependent protein binding, and cell adhesion molecule binding (Fig. 4A-C).

In the KEGG pathway analysis, the enriched pathways included the PI3K-Akt signaling pathway and ECM-receptor interaction in metabolism, endocytosis, regulation of actin cytoskeleton, focal adhesion, and cell adhesion molecules in cellular processes (Fig. 4D). The enriched

Table 5
Detailed clinical information from 11 patients.

Patient number	Gender	Age	CEA (ng/ml)	CA199 (ng/ml)	Tumor site	Tumor size (cm)	Tumor pattern	Pathological type	IHC	Metastasis (liver/lung/ascites)	Lymph node metastasis	TNM stage	Stage
Patient 1	Female	45	5.38	5.38	Carcinoma of the straight B junction	4.5 × 5	Ulcerative	Moderately and poorly differentiated tubular adenocarcinoma	EGFR(Membranous plasma+); Ki-67(+30%);p53(Missense mutation);MLH-1(+); MSH-2(+); MSH-6(+); PMS-2(+)	no	241(4/12)	pT4bN2M0	IIIC
Patient 2	Female	77	6.1	5.76	Upper rectum	6.5 × 4.3	Ulcerative	Moderately and well differentiated tubular adenocarcinoma with papillary adenocarcinoma	EGFR(Membrane weak+); Ki-67(+70%); p53(Mutation); MLH-1(+); MSH-2(+); MSH-6(+); PMS-2(+)	no	no	pT4aN0M0	IIB
Patient 3	Male	63	3.07	2.5	Sigmoid colon	2.3 × 2.1	Uplift	Moderately differentiated tubular adenocarcinoma	EGFR(Membrane +); Ki-67(+20%);p53(Nonsense mutation);MLH-1(+); MSH-2(+); MSH-6(+); PMS-2(+)	no	no	pT2N0M0	I
Patient 4	Female	63	3.55	12.17	Carcinoma of the straight B junction	5.5 × 5	Ulcerative	Moderately differentiated tubular adenocarcinoma	EGFR(Membrane weak+); Ki-67(+70%); p53(Mutation); MLH-1(+); MSH-2(+); MSH-6(+); PMS-2(+)	no	no	pT3N0M0	IIA
Patient 5	Female	65	1.41	9.06	Ascending colon	7.3 × 5	Ulcerative	Moderately differentiated tubular adenocarcinoma with mucinous adenocarcinoma	EGFR (Membranous plasma+); Ki-67(+60–70%); p53(+30%); MLH-1(+); MSH-2(+); MSH-6(+); PMS-2(+)	no	201(1c);202(1c)	pT3N1cM0	IIIB
Patient 6	Male	75	46.88	16.35	Low rectum	6 × 3.5	Ulcerative	Moderately and poorly differentiated tubular adenocarcinoma	EGFR (most membranous plasma+); Ki-67(+80%); p53(+,mutation) MLH-1(+); MSH-2(+); MSH-6(+); PMS-2(+)	no	251(13/16); 252(3/3)	pT4aN2M0	IIIC
Patient 7	Female	65	2.14	46.5	Low rectum	4.5 × 3.5	Uplift	粘液腺癌 (侵透肌层, 侵及肌层外纤维组织, 未见明确神经侵犯)	EGFR (+); Ki-67(+60%); p53(90%+, mutation); MLH-1(+); MSH-2(+); MSH-6(+); PMS-2(+)	no	251(1/9 + 1c);252(1/6)	pT4aN2M0	IIIC
Patient 8	Female	69	9.74	0.74	Hepatic flexure of colon	5 × 3.5	Ulcerative	Mucinous adenocarcinoma	EGFR (+); Ki-67(+70%); p53(95%+, mutation); MLH-1(+); MSH-2(+); MSH-6(+); PMS-2(+)	no	221(1/11);223(1/2)	pT4aN0M0	IIB
Patient 9	Male	79	7.29	6.09	Ascending colon	4.5 × 3	Ulcerative	Papillary adenocarcinoma with moderately differentiated tubular adenocarcinoma	EGFR (plasma+); Ki-67(+80%); p53(+,mutation)MLH-1(+); MSH-2(+); MSH-6(+); PMS-2(+)	no	211(1/5)	pT4aN1M0	IIIB
Patient 10	Female	67	0.76	8.1	Low rectum	1.5 × 1.5	Uplift	Papillary adenocarcinoma with well and moderately differentiated tubular adenocarcinoma	EGFR (Membrane weak+); Ki-67(+70%); p53(Missense mutation); MLH-1(+); MSH-2(+); MSH-6(+); PMS-2(+)	no	no	pT1N0M0	I
Patient 11	Female	60	3.21	8.89	Low rectum	4 × 3	Ulcerative	Poorly differentiated tubular adenocarcinoma	EGFR(Membranous plasma+); Ki-67(+80%); p53(weak or strong+70%); MLH-1(+); MSH-2(+); MSH-6(+); PMS-2(+)	no	no	pT2N0M0	I

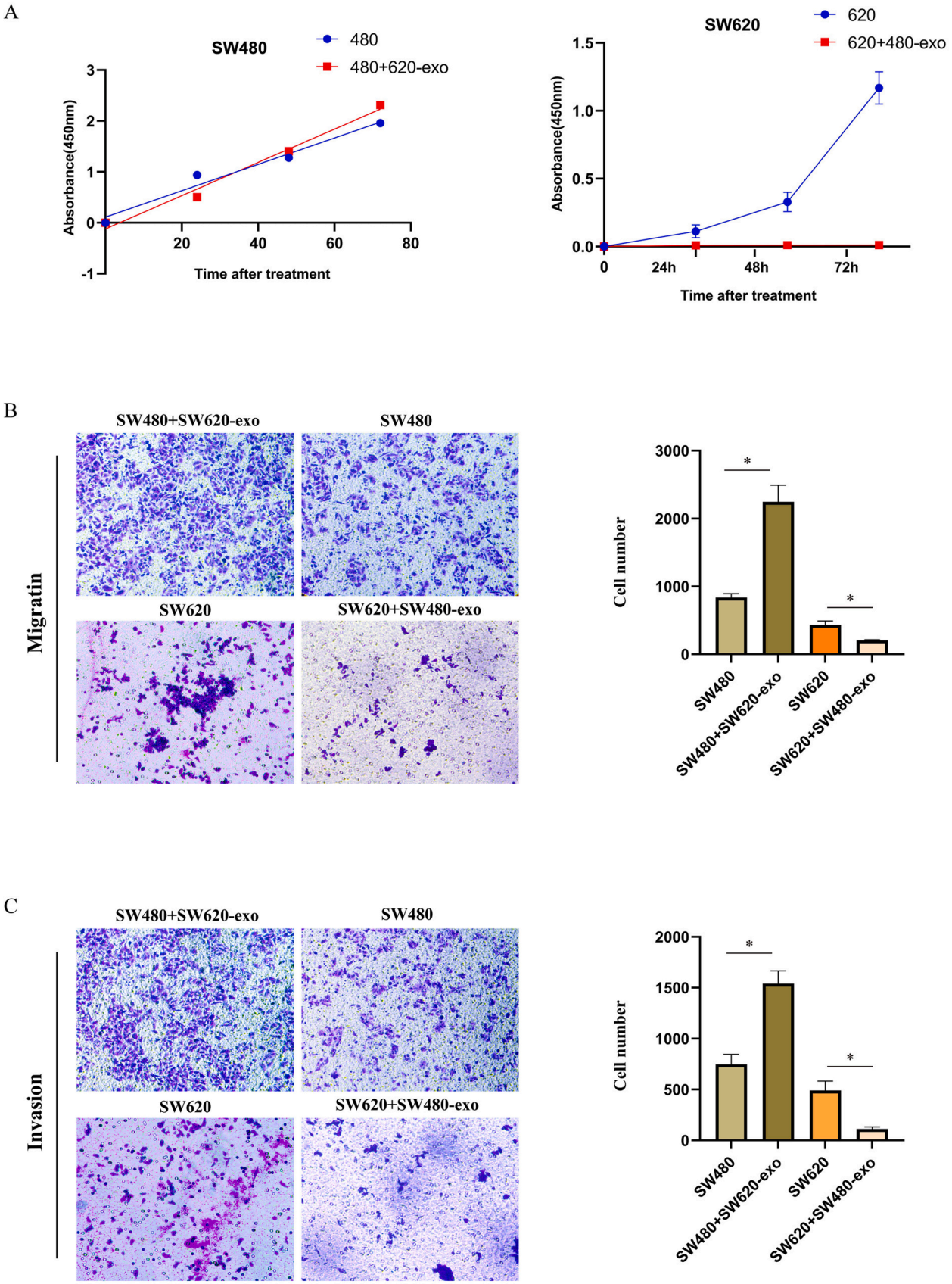

Fig. 3. . The changes in the migration and invasion ability of CRC cells after treated with SW620-exo and SW480-exo. (A) SW620-exo enhanced proliferation of SW480 cells and SW480-exo inhibited proliferation of SW620 cells by CCK-8 analysis. (B) SW620-exo enhanced migration of SW480 cells by Transwell invasion assay. (C) SW620-exo enhanced invasion of SW480 cells by Transwell invasion assay. ($P < 0.05$, Student's *t*-test) (*p, 0.05).

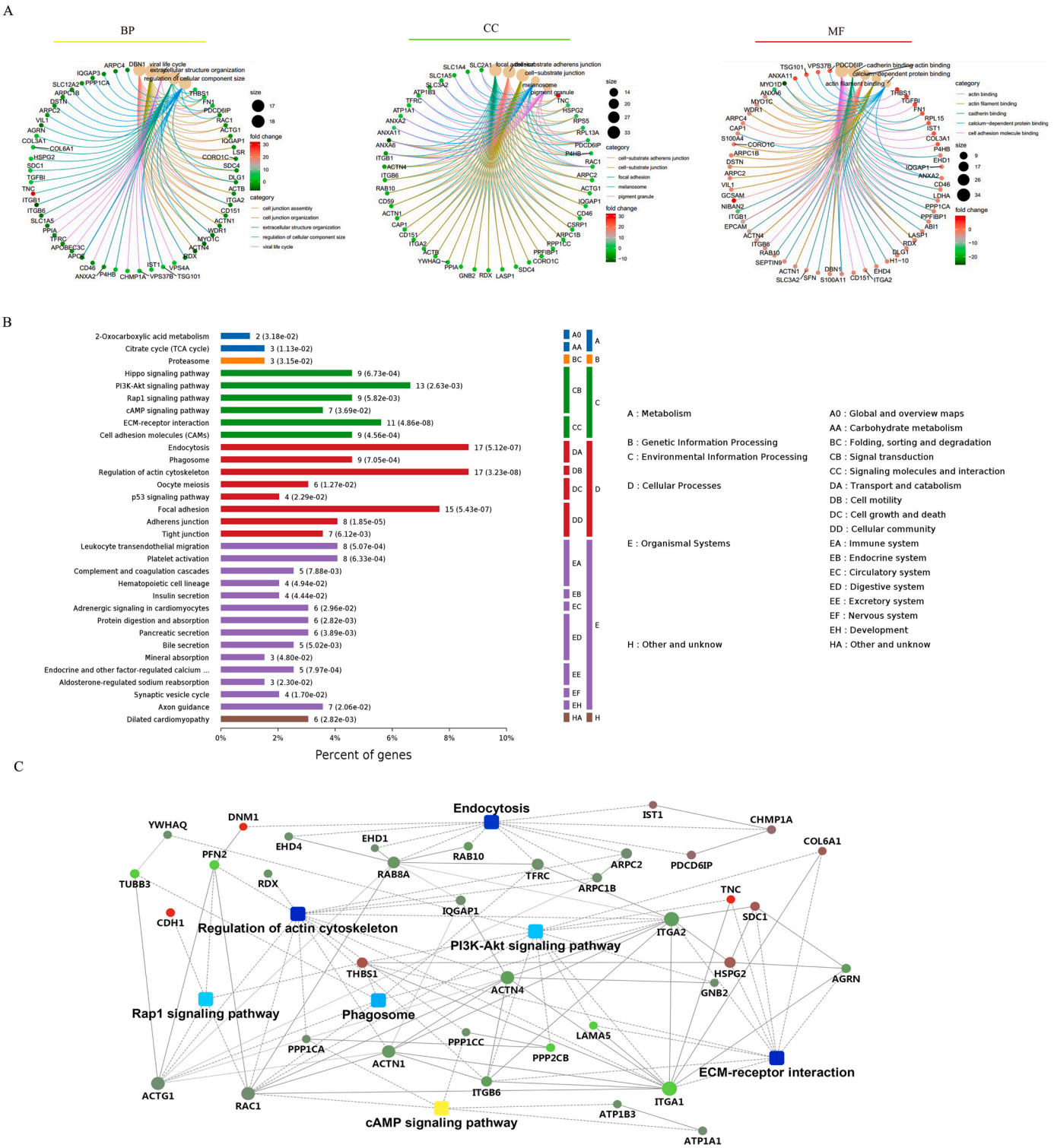

Fig. 4. Bioinformatics analysis of upregulated and downregulated exoDEPs. (A) GO annotation includes Biological Processes (BP), Cellular component (CC) and Molecular Function (MF) analysis. Coloring of proteins is based on functional enrichment analysis; (B) The enriched pathways by KEGG analysis; (C) Visible clusters of the protein-protein interaction map was assigned to enriched ontologies among the upregulated and downregulated exoDEPs with calculated P-value adjusted for multiple comparisons.

pathways suggest that the exosomal proteins were mostly active in the process of tumor metabolism, cellular movement, and skeleton connection in the microenvironment.

To identify the chief nodes and important connectors among the exoDEPs, we performed the PPI network analysis using Cytoscape 3.8.2. There were 114 exoDEPs that had at least one known interaction with other proteins in the PPI network ($P < 1.0e-16$). The top 20 active proteins with three or more interactions were PS1TP5BP1, GAPDH, ACTG1, FN1, ITGB1, RAC1, ACTN4, TSG101, ACTN1, TFRC, ITGA2, ANXA2, THBS1, SDC1, LDHA, APOE, P4HB, HSPG2, MYO1C, and ARPC2. These proteins were mostly associated with pathways including endocytosis, regulation of actin cytoskeleton, Rap1 signaling pathway,

cAMP signaling pathway, and PI3K-Akt signaling pathway. The direct interactions between these highly active proteins and enriched pathways are also shown in Fig. 4E.

Bioinformatics analysis of "all or none" exoDEPs

For the "all or none" exoDEPs, GO annotation, KEGG pathway, and PPI network analysis were carried out separately. For biological process classification, exoDEPs expressed only in SW620 are mainly associated with the regulation of synapse structure or activity, synapse organization, response to amyloid-beta, positive regulation of intracellular protein transport, and positive regulation of cellular protein localization. ExoDEPs expressed only in SW480 cells are mainly associated with cell-substrate adhesion, cell-matrix adhesion, positive regulation of interleukin-8 production, negative regulation of the canonical Wnt-signaling pathway, and regulation of hair follicle development. For cellular components, exoDEPs expressed only in SW620 were mainly associated with glutamatergic synapse, endoplasmic reticulum lumen, clathrin-coated pit, interstitial matrix, and glial cell projection. ExoDEPs expressed only in SW480 are mainly associated with focal adhesion, cell-substrate adherens junction, cell-substrate junction, collagen-containing extracellular matrix, and proteasome regulatory particles. For molecular function, exoDEPs expressed only in SW620 were mainly associated with amide binding, clathrin binding, glycosaminoglycan binding, peptide binding, and signal sequence binding, while exoDEPs expressed only in SW480 were mainly associated with actin monomer binding, cadherin binding, cell adhesion mediator activity, cell adhesion molecule binding, and proteasome binding (Fig. 5A).

For the KEGG pathway analysis, exoDEPs expressed only in SW620 were mostly active in pathways including the adherens junction, endocrine and other factor-regulated calcium reabsorption, endocytosis, focal adhesion, and phospholipase D signaling pathway. ExoDEPs expressed only in SW480 were mostly active in pathways including Epstein-Barr virus infection, citrate cycle (TCA cycle), Huntington

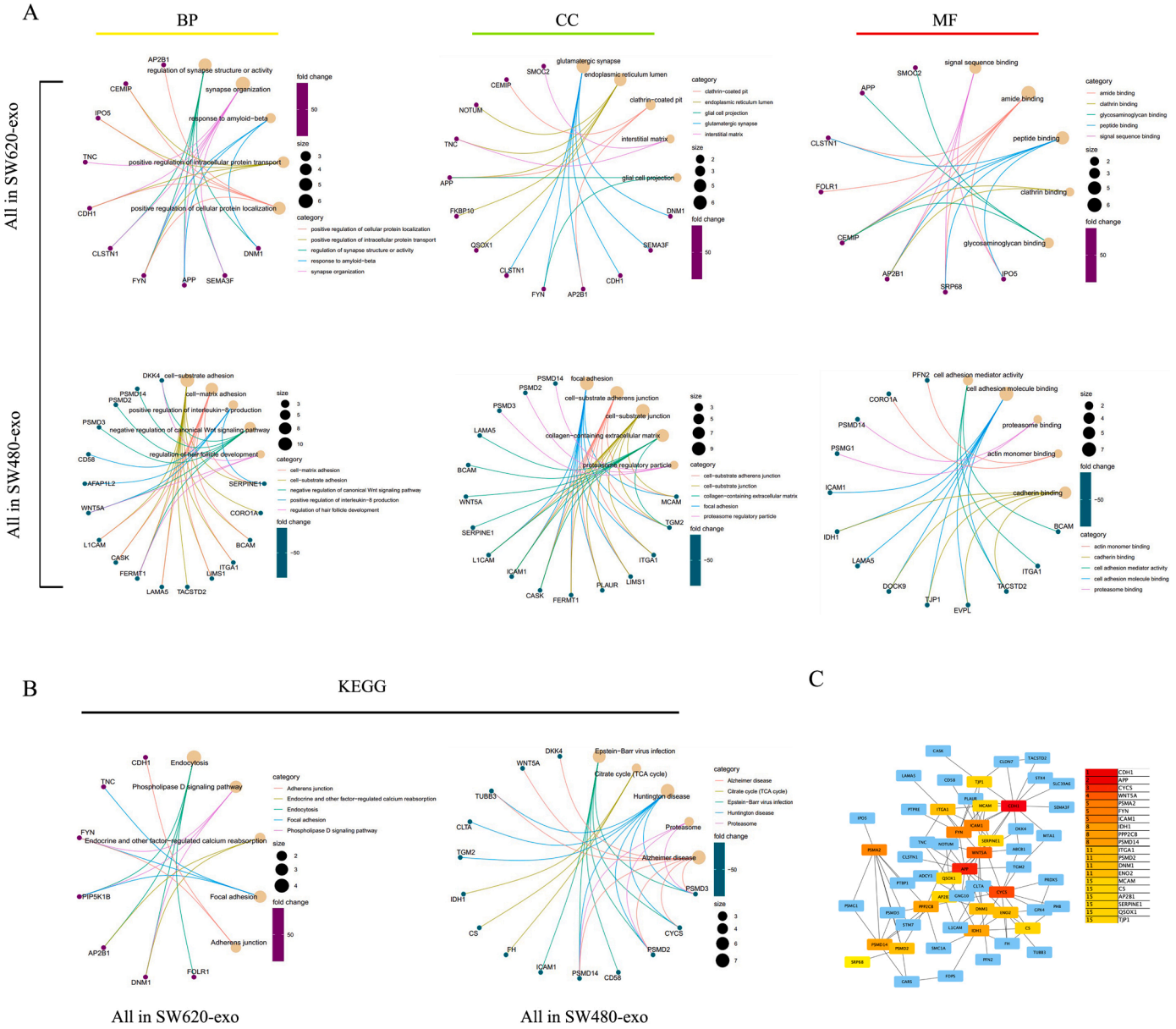

Fig. 5. Bioinformatics analysis of "all or none" exoDEPs. (A) GO annotation includes Biological Processes (BP), Cellular component (CC) and Molecular Function (MF) analysis. Coloring of proteins is based on functional enrichment analysis; (B) The enriched pathways by KEGG analysis; (C) Visible clusters of the protein-protein interaction map was assigned to enriched ontologies among the "all or none" exoDEPs with calculated P-value adjusted for multiple comparisons.

disease, proteasome, and Alzheimer disease (Fig. 5B).

In the PPI network analysis, 88 exoDEPs had at least one known interaction with other proteins in the PPI network (P = 5.08e-07) (Fig. 5C). The top 20 active proteins with three or more interactions were CDH1, APP, CYCS, WNT5A, PSMA2, FYN, ICAM1, IDH1, PPP2CB, PSMD14, ITGA1, PSMD2, DNM1, ENO2, MCAM, CS, AP2B1, SERPINE1, QSOX1, and TJP1. These proteins were mostly associated with pathways including 2-oxocarboxylic acid metabolism, citrate cycle (TCA cycle), proteasome, synaptic vesicle cycle, endocrine and other factor-regulated calcium reabsorption, pathogenic *Escherichia coli* infection, viral myocarditis, cell adhesion molecules (CAMs), phospholipase D signaling pathway, carbon metabolism, apelin signaling pathway, and Epstein-Barr virus infection.

In summary, metabolism and cell movement regulation are the main

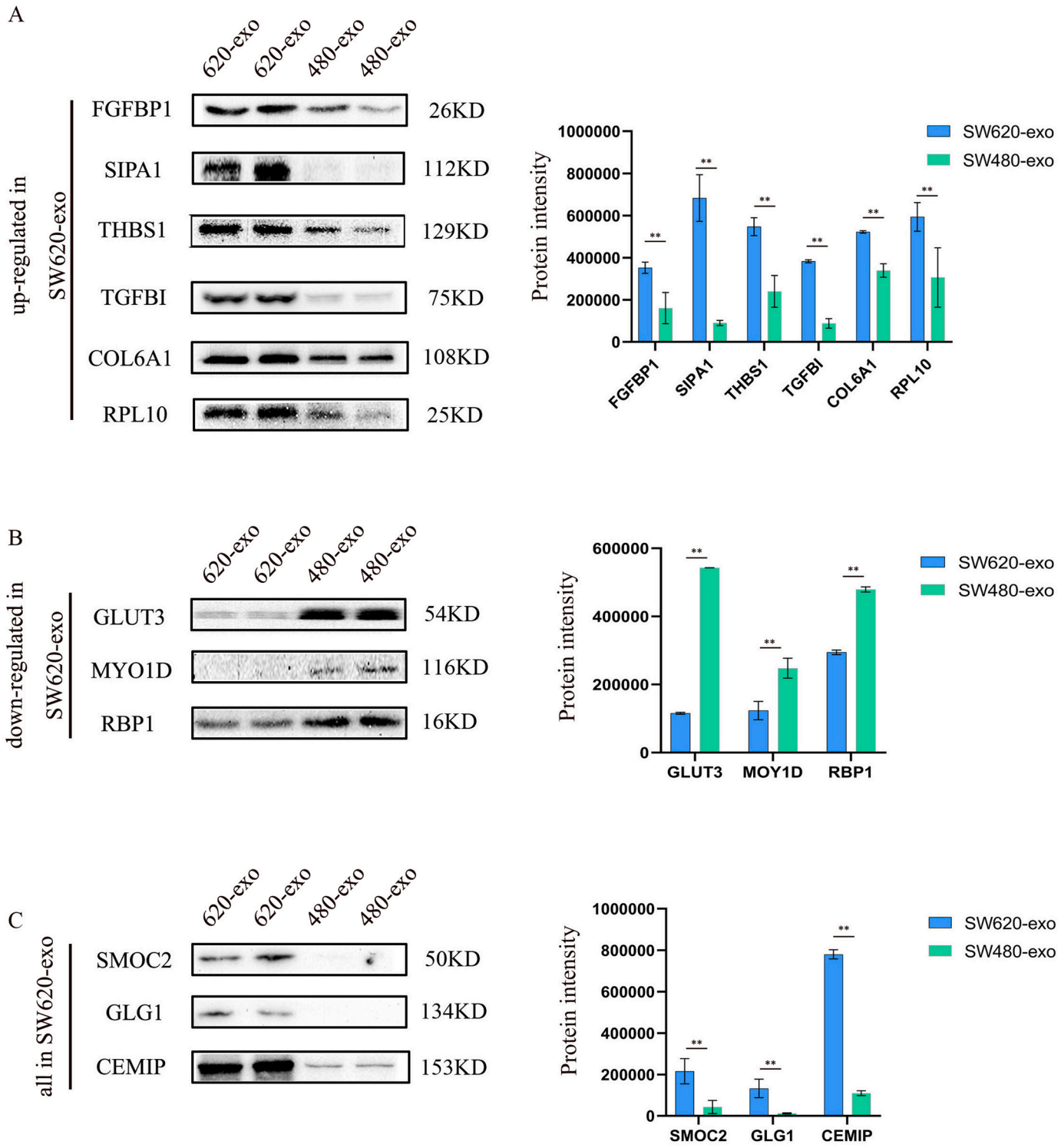

Fig. 6. Validation of exoDEPs by WB on CRC cell line exosomes. (A) Six upregulated proteins FGFBP1, SIPA1, THBS1, TGFBI, COL6A1, and RPL10 were verified overexpressed in SW620 exosomes. (B) Three downregulated proteins GLUT3, MYO1D, and RBP1 were verified to be overexpressed in SW480 exosomes. (C) Three proteins SMOC2, GLG1 and CEMIP were verified to be obviously overexpressed in SW620 exosomes. (P, 0.05, Student's *t*-test) (*$p < 0.05$, **$p < 0.01$).

mechanisms involved in "all or none" exoDEPs. Compared to the exosomes of SW620, the proteins that disappeared in the exosomes of SW480 may play a role and may degrade or they may be transmitted as messengers. These proteins play an important role in the invasion and metastasis of CRC.

Validation of exoDEPs by WB on CRC cell line exosomes

To obtain independent evidence for exoDEPs identified by label-free proteomics, we chose six upregulated proteins, three downregulated proteins, and three proteins only expressed in SW620 for verification by WB. The results showed that six upregulated proteins, FGFBP1, SIPA1, THBS1, TGFBI, COL6A1, and RPL10 were overexpressed in the SW620 exosomes (Fig. 6A) and three downregulated proteins, GLUT3, MYO1D, and RBP1, were overexpressed in SW480 exosomes (Fig. 6B). Three proteins expressed in SW620 exosomes, namely SMOC2, GLG1, and CEMIP, were verified as overexpressed in the SW620 exosomes (Fig. 6C). However, the differences in expression identified by WB were not coordinated with mass spectrometry. In the verification of the upregulated proteins, the expression differences of SIPA1 and TGFBI were the most obvious and not FGFBP1. The differences in the expression of THBS1 and COL6A1 were not obvious as in mass spectrometry. In the verification of SMOC2, GLG1, and CEMIP that were expressed only in SW620, both SMOC2 and GLG1 showed little expression in SW480 exosomes, while the expression of CEMIP in SW480 exosomes could still be seen.

Validation of exoDEPs by IHC on clinical human CRC pathologic tissues

In this study, we chose six upregulated exoDEPs, FGFBP1, SIPA1, THBS1, TGFBI, COL6A1, and RPL10; three downregulated exoDEPs, GLUT3, MYO1D, and RBP1 in SW620; and three exoDEPs, SMOC2, GLG1, and CEMIP, that were expressed only in SW620 for verification by IHC staining of compared non-lymph node metastatic ($n = 6$) and lymph node metastatic CRC tissues ($n = 5$) (Fig. 7).

The results indicated that six upregulated exoDEPs, namely FGFBP1, SIPA1, THBS1, TGFBI, COL6A1, and RPL10, were overexpressed in CRC tissues with lymph node metastasis, and three downregulated exoDEPs, namely GLUT3, MYO1D, and RBP1, were overexpressed in CRC tissues without lymph node metastasis. Three exoDEPs expressed only in SW620, namely SMOC2, GLG1 and CEMIP, were found to be overexpressed in CRC tissues with lymph node metastasis. Most proteins are expressed in tissues between tumors rather than in cells. Compared with the expression in cancer tissues, the expression levels of all identified exoDEPs in paracancerous tissues were lower. The immunostaining densities of proteins were quantitatively assessed using NIS-Elements BR 3.0 (Nikon, Tokyo, Japan). In brief, after placing the sections on a microscope (Nikon E800), the images were transferred to a computer using a digital camera (Nikon 80i). Three visual fields were randomly examined on all slides under high-power magnification. The mean optical densities of the positive areas were measured. The results were expressed as the exact values of the relative optical density units. This analysis confirmed that all three proteins were significantly upregulated in both non-metastatic and metastatic CRC tissues.

Discussion

Exosomes are nanovesicles that play a major role in the TME, especially in cell-cell communication by horizontal transfer of signaling molecules. TME-derived exosomes also support metastatic niche formation, suppress the antitumor immune response, and impart drug resistance. Our proteomic analysis aimed to reveal the exosomal proteins that affect CRC invasion and metastasis. In this study, we used a label-free proteomics method to perform comparative proteomic analysis of exosomes from a pair of homologous human CRC cell lines SW620 (highly metastatic) and SW480 (weakly metastatic), which have different metastatic abilities. A total of 942 exoDEPs were quantified, among which 115 exoDEPs (31 upregulated and 84 downregulated in SW620 exosomes) showed obvious differential expression (2.0-fold change, $P < 0.05$). The total 90 "all or none" exoDEPs were identified in this analysis, wherein 30 proteins were found expressed only in SW620 exosomes, and 60 proteins were found expressed only in SW480 exosomes.

To verify the data obtained in this research, we chose six upregulated exoDEPs in SW620, including FGFBP1, SIPA1, THBS1, TGFBI, COL6A1, and RPL10 and subjected them to WB and IHC. All six proteins were upregulated in SW620 exosomes and CRC tissues with metastasis. The expression of the six proteins correlated with poor pathological type and late stage.

Fibroblast growth factor-binding protein 1 (FGFBP1) was the first upregulated exoDEP in SW620 cells. It is a secreted chaperone that mobilizes paracrine-acting FGFs, stored in the extracellular matrix, and presents them to their cognate receptors. Several studies have demonstrated FGFBP1 overexpression in various tumors, including head and neck squamous cell carcinoma (HNSCC), mammary, cervix, prostate, melanoma, colon, and pancreatic cancer [10–13]. In previous studies, the role of FGFBP1 was mostly related to cancer cell proliferation and angiogenesis. Recent studies have indicated the promoting metastatic role of FGFBP1. HSD11B2 was reported to enhance CRC cell migration and invasion capacity by upregulating the expression by FGFBP1, increasing the phosphorylation of AKT in the PI3K-Akt pathway [14]. FGFBP1 also acts as a downstream target of the FBW7/c-Myc axis and promotes cell proliferation and migration in pancreatic cancer [15]. There are no reports on the exosomal role of FGFBP1 in tumor progression. In this study, we verified the upregulation of exo-FGFBP1 in a highly metastatic CRC cell line. The results confirmed the positive exosomal role of FGFBP1 in the invasion and metastasis of CRC cells from the TME. However, the understanding of the specific mechanism requires further study.

Signal-induced proliferation associated protein 1 (SIPA1) is the third most upregulated exoDEP in SW620 cells. It is a GTPase-activating protein expressed in proliferative active lymphoid cells as a mitogen-induced nuclear protein. SIPA1 has a tight interaction in controlling cellular adhesion in cancer metastasis [16]. Overexpression of SIPA1 was found in colon, prostate, breast, and other several types of cancers [17,18]. SIPA1 promotes cancer metastasis by inhibiting adhesion and downregulating the expression of ECM-related proteins [19]. The findings of this study verified the metastasis-promoting role of SIPA1 as an exosomal protein in the CRC microenvironment. IHC results indicated that SIPA1 was mostly expressed in the tissue around or between cancer cells. Combined with other research results, exo-SIPA1 may be secreted to decrease intercellular adhesion in the CRC.

Thrombospondin-1 (THBS1) is the fifth most upregulated exoDEP in SW620 cells. As a glycoprotein, it is an endogenous inhibitor of angiogenesis and tumor progression. Downregulation of THBS1 is reported to be correlated with poor prognosis in lung, breast, and cervical cancer [20–22]. For THBS1 and CRC, a recent study indicated that low THBS1 expression correlated with late stage of liver and lymph node metastasis and significantly worse overall survival rate than high THBS1 expression [23]. Although most results indicated the negative role of THBS1 in tumor progression, we verified the upregulation of THBS1 in highly metastatic CRC cell line exosomes. This result appears to be more complicated. The role of THBS1 as an exosome in the extracellular microenvironment is contrary to its role in the cell. In previous studies, the positive role of exo-THBS1 in CRC invasion and metastasis has rarely been confirmed. This special finding may provide new research directions for THBS1 in the CRC microenvironment.

Transforming growth factor β-induced protein (TGFBI) is the sixth most upregulated exoDEP in SW620 cells. It is a secreted extracellular matrix protein consisting of 683 amino acids and includes four evolutionarily conserved fasciclin-1 domains and a C-terminal Arg-Gly-Asp motif [24]. The role of TGFBI in cancer is unclear. It appears to be tissue-specific, acting as a tumor suppressor or promoter.

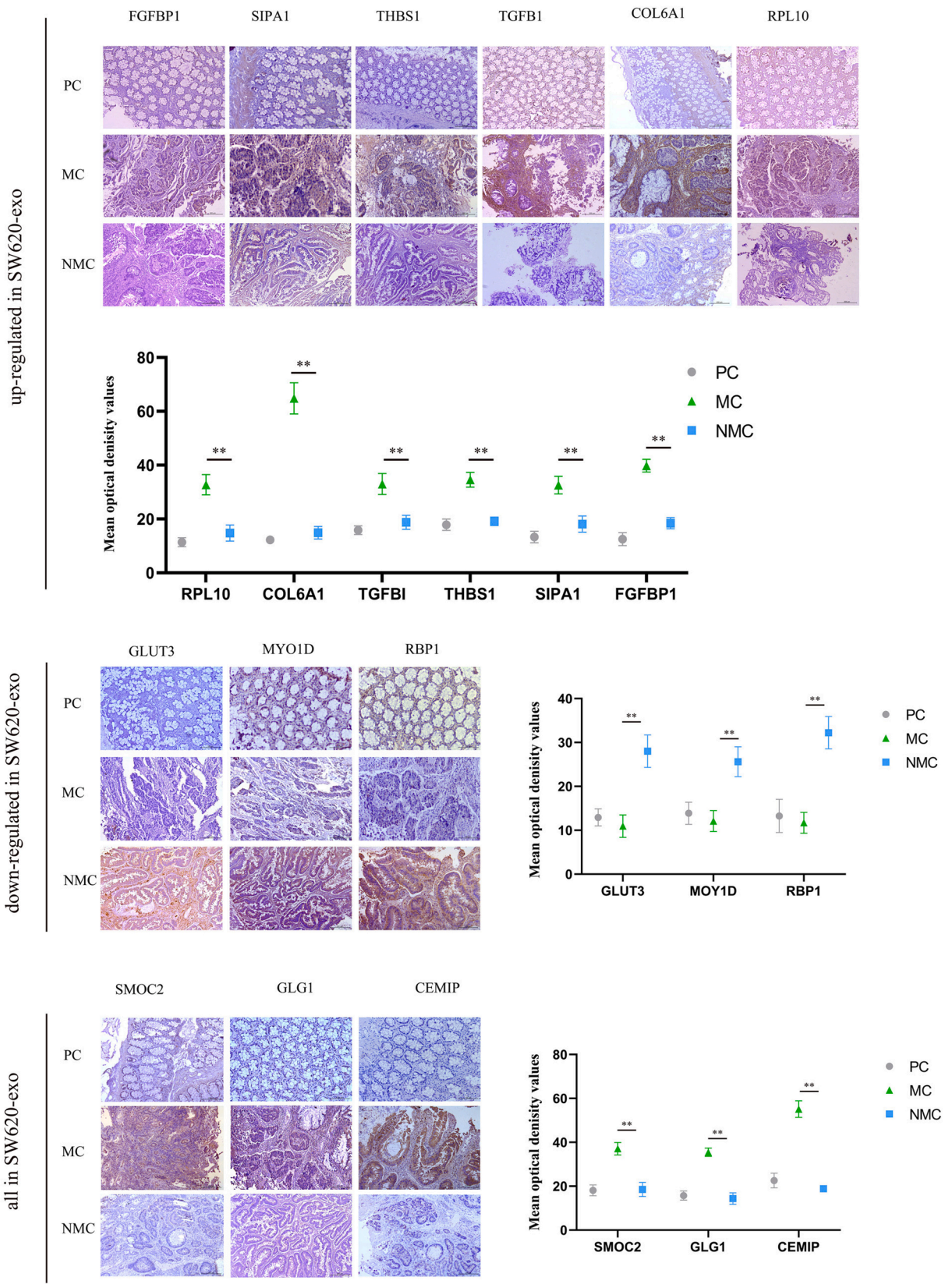

Fig. 7. Validation of exoDEPs by IHC on clinical human CRC pathologic tissues. (A) Six upregulated proteins FGFBP1, SIPA1, THBS1, TGFBI, COL6A1, and RPL10 were found to be overexpressed in CRC tissues with lymph node metastasis. (B) Three downregulated proteins GLUT3, MYO1D, and RBP1 were found to be overexpressed in CRC tissues without lymph node metastasis. (C) Three proteins SMOC2, GLG1, and CEMIP were verified obviously overexpressed in CRC tissues with lymph node metastasis. (P,0.05, Student's *t*-test) (*$p < 0.05$, **$p < 0.01$).

Downregulation of TGFBI was observed in leukemia [25], whereas hypermethylation of the TGFBI promoter, which suppresses TGFBI expression, was observed in ovarian, prostate, and lung carcinomas [26,27]. These findings indicated the tumor-suppressor functions of TGFBI. Conversely, TGFBI is also known to perform tumor promoter functions in various cancers. TGFBI upregulation has been reported as a promising prognostic marker in oral squamous cell carcinoma, renal cell carcinoma, and pancreatic cancer [28]. In this study, we verified the promoting role of TGFBI in the invasion and metastasis of CRC as an exosome, which has not been previously reported. The exosomal role of TGFBI is very promising and requires further study.

Collagen type VI α1 chain (COL6A1) is another upregulated exoDEP and has an anchoring function that plays roles in cell migration, differentiation, and embryonic development [29]. Compared to the corresponding normal tissues, COL6A1 is more active in tumor tissues such as cervical cancer, prostate cancer, and lung cancer [30,31]. Overexpression of COL6A1 enhances the motility and metastasis of cancer cells [32]. Although the role of COL6A1 has been elucidated, its role as an exosome has seldom been determined.

Ribosomal protein L10 (RPL10), also known as UL16, is a 25 kDa protein, which was first found in non-tumorigenic Wilms tumors, and participates in the late steps of 60S ribosomal assembly [33]. RPL10 mainly plays a role in protein synthesis. However, an increasing number of studies have shown that RPL10 also has ribose functions in vitro, such as participating in signaling pathways in different cell biological processes, regulating cell proliferation, migration, and differentiation. In terms of tumor, some studies have confirmed that the expression level of RPL10 in human epithelial ovarian cancer is higher than that in normal ovarian tissue. When its expression level decreases, the viability, migration, and invasion ability of epithelial ovarian cancer cells decrease, but the apoptosis level increases [34]. Similarly, in a study of prostate cancer, high levels of RPL10 expression can promote the progression of advanced tumors [35,36]. Tumor immunity has been a promising research direction in recent years. Proteomic studies have shown that RPL10 can participate in the JAK/STAT signaling pathway and promote the progression of T-lymphocytic leukemia [37]. Our research also confirmed the promoting role of exo-RPL10 in CRC metastasis. Based on the above results, we speculate that RPL10 may have a function beyond the ribosome, such as immunosuppression in the process of tumor development.

The top three downregulated exoDEPs in SW620, including SLC2A3, MYO1D, and RBP1, were also verified. They were upregulated in SW620 exosomes and CRC tissues without metastasis. The overexpression of the three proteins demonstrated a correlation with the pathological type and early stage.

Solute carrier family 2 member 3 (SLC2A3), also known as GLUT3, facilitates glucose transport. In previous research, tumors with high expression of SLC2A3 were shown to enrich immune cell infiltration in the TME. An association between the overexpression of SLC2A3 and poor clinical outcomes has been reported in CRC [38,39]. In Yao's research, SLC2A3 accelerated aerobic glycolysis in gastric cancer cells by activating the SLC2A3-STAT3-SLC2A3 feedback loop and then promoting phosphorylation of the STAT3 signaling pathway and downstream glycolytic targeting gene. SLC2A3 also potentially contributes to the M2 subtype transition of macrophage infiltration in the gastric cancer microenvironment [40]. However, in our study, exo-SLC2A3 was found to inhibit the malignant behavior of CRC metastasis. The opposite role of intracellular and extracellular is a valuable part of this study and warrants further research.

Unconventional myosin-1d (MYO1D) belongs to the EGFR family (except ErbB3) at the plasma membrane. It binds only with unphosphorylated EGFRs and anchors them to the underlying actin cytoskeleton at the plasma membrane. Overexpression of MYO1D enhances colorectal and breast cancer cell motility and viability by upregulating EGFR levels, thereby promoting colorectal tumor progression in vivo in mice. MYO1D is upregulated in human CRC tissues from the advanced stages. Overexpressed MYO1D contributes to CRC, possibly as a novel oncogene, thus serving as an additional target for the suppression of RTK signaling. However, in this study, exo-MYO1D in the microenvironment might play an inhibitory role in the malignant behavior of CRC. The detailed mechanism requires further verification and study.

Retinol-binding protein 1 (RBP1) is a cytosolic carrier that regulates retinol homeostasis in various human and rodent tissues [41,42]. It possesses high-affinity binding of retinoic acid and possibly functions as a chaperone-like protein to regulate the prenuclear phase of retinoic acid signaling [43,44]. Studies have reported that RBP1 is abnormally expressed in several human cancers, including bladder cancer, laryngeal cancer, and tongue squamous cell carcinoma [45–47]. RBP1 overexpression promotes cell autophagy in OSCC cells by interacting with CKAP4 [48]. However, in this study, exo-RBP1 in the microenvironment might play an inhibitory role in the malignant behavior of CRC. The detailed mechanism requires further verification and study.

In our research, the discovery of the "all or none" exoDEPs was of great significance. The exoDEPs expressed only in SW620 cells can more clearly show their ability to promote the invasion and metastasis of CRC cells. We screened out ninety "all or none" exoDEPs, including 30 ones only expressed in SW620 and 60 ones only expressed in SW480. Among these exoDEPs, we performed WB and IHC experiments using SMOC2, GLG1, and CEMIP to verify the results of proteomics. Overexpression of the three proteins demonstrated a correlation with the late pathological stage.

Secreted modular calcium-binding protein2 (SMOC2) belongs to the secreted protein acidic and rich in cysteine (SPARC) family of matricellular proteins. It regulates the expression of ECM and Matrix metalloproteinases (MMPs) and modulates cell-matrix interactions, focal adhesion, and actin stress fiber organization by activating cellular integrins [49]. The expression and functional significance of SMOC2 have been explored in many types of cancers, such as breast, colon, lung, and liver cancers [49–52]. As an intestinal stem cell marker, SMOC2 elevation is necessary to increase cell motility, proliferation, and liver metastasis in colon cancer. However, in a recent study by Jang, SMOC2 was suggested as an independent prognostic marker for better clinical outcomes in a large cohort of CRC patients and acts as a tumor suppressor in CRC progression [53]. In this study, we confirmed that SMOC2 promotes the invasion and metastasis of CRC as an exosome and from the extracellular perspective. Therefore, combined with these controversial results, the role of exo-SMOC2 is largely unknown and needs to be further explored.

Golgi glycoprotein 1 (GLG1, also called E-selectin Ligand 1, Esl1) is a cysteine-rich fibroblast growth factor receptor (FGFR). GLG1 has been reported to be associated with the progression of various carcinomas. FGFR signaling possesses broad mitogenic and cell survival mechanisms and is involved in a variety of biological processes, including embryonic development, cell growth, and tumor invasion [54]. In a study by Tamami Morisaki, GLG1 was found to be significantly associated with the T stage with respect to invasion depth [55]. It should be noted that GLG1 may be associated with the invasion potential of CSCs via FGFR signaling.

CEMIP, also known as KIAA1199 (cell migration-inducing protein), is a secreted protein that plays a role in extracellular ligand binding and processing. The biological role of CEMIP has been studied in cancer biology, and a number of studies have demonstrated its high expression levels in cancer cell lines and its association with cancer invasion and

metastasis [56,57]. It plays a crucial role in the apoptosis, proliferation, invasion, and migration of various cancer cells. In addition, CEMIP is also involved in the regulation of various signaling pathways such as epithelial-mesenchymal transition (EMT), PI3K/Akt, MEK/ERK, and Wnt/β-catenin. In CRC research, CEMIP was found to be significantly overexpressed in the adenoma-adenocarcinoma pathway of colorectal carcinogenesis [58]. CEMIP mRNA was also detected in the plasma of patients with colorectal neoplasia than in the plasma from healthy controls [59]. These results suggest that CEMIP is both an endogenous and a secreted protein in the CRC. However, its role in promoting cancer cell metastasis as an exosome has not been extensively studied.

Reviewing the whole study, we think that there are some limitations that need to be improved. First, the clinical sample volume is limited, and a larger clinical sample volume collected is needed in the future study to establish the reference of clinical features. Second, the validated exoDEPs may play an important regulatory role in the progress of CRC, therefore, elucidation of deeper mechanism research is needed in future study.

In conclusion, in this study, we first found that SW620-derived exosomes could significantly enhance the proliferation, migration and invasion abilities of SW480 cells. These results indicated that highly invasive colorectal cancer cells may transport their oncogenic characteristics to less invasive cancer cells through the exosomes to accelerate disease progression. We then used a label-free proteomics as a large-scale purification method to compare this pair of homologous CRC cell lines with different metastatic abilities to reveal the most associated exosomal proteins regulating CRC metastasis. Finally, six upregulated exoDEPs (FGFBP1, SIPA1, THBS1, TGFBI, COL6A1, and RPL10), three downregulated exoDEPs (SLC2A3 [GLUT3], MYO1D, and RBP1), and three exoDEPs (SMOC2, GLG1, and CEMIP) expressed only in SW620 were validated by western blot (WB) and immunohistochemistry (IHC). Verification of these exosomal proteins revealed their potential biochemical characteristics and regulatory functions in CRC invasion and metastasis.

Author contributions

Xinlu Liu and Ge Liu; Methodology, Xinlu Liu and Na Li; Software, Xinlu Liu; Validation, Xinlu Liu, Na Li, Chi Zhang and Xiaoyu Wu; Formal Analysis, Xinlu Liu and Na Li; Data Curation, Xinlu Liu, Na Li, Chi Zhang, Xiaoyu Wu, Gang Dong and Shoujia Zhang; Writing – Original Draft Preparation, Xinlu Liu; Writing – Review & Editing, Xinlu Liu, Na Li and Chi Zhang; Visualization, Xinlu Liu; Supervision, Xinlu Liu and Ge Liu.

Funding

There is no funding for this research.

Supplementary Tables

Table S1

Protein IDs	Protein names	Gene names	Sequence coverage [%]	Mol. weight [kDa]	SW620/ SW480	P. value
Q14512	Fibroblast growth factor-binding protein 1	FGFBP1	19.2	26.264	35.5622503	0.03006523
P24821	Tenascin	TNC	31.2	240.85	31.9171121	0.02235115
Q96FS4	Signal-induced proliferation-associated protein 1	SIPA1	0.7	101.82	13.2653467	0.00628316
Q8N6F7	Galanin peptides	GAL	25.2	13.302	6.59087605	0.00043934
P07996	Thrombospondin-1	THBS1	25.7	129.38	5.15722985	0.00596742
Q15582	Transforming growth factor-beta-induced protein ig-h3	TGFBI	26.4	74.68	4.29955673	0.00079523
Q08380	Galectin-3-binding protein	LGALS3BP	30.4	65.33	4.23649295	0.02398548
P18827	Syndecan-1	SDC1	10.6	16.936	3.95082411	0.00969672
P98160	Basement membrane-specific heparan sulfate proteoglycan core protein	HSPG2	31.7	464.01	3.65451637	0.00490496
P50995	Annexin A11	ANXA11	39.7	45.597	3.63266542	0.00082676
P46782	40S ribosomal protein S5	RPS5	16	22.391	3.43144522	0.0340731
P67809	Y-box-binding protein	YBX1	16.5	29.374	3.11206098	0.03244381
P02751	Fibronectin	FN1	27.8	259.21	3.06819854	0.03725025
P12109	Collagen alpha-1(VI) chain	COL6A1	3.8	108.34	3.06807273	0.00024771
Q9UN37	Vacuolar protein sorting-associated protein 4A	VPS4A	16.7	26.829	2.70042167	0.00500222
Q9P265	Disco-interacting protein 2 homolog B	DIP2B	7.1	171.49	2.68856637	0.0007878
P46779	60S ribosomal protein L28	RPL28	21.3	9.657	2.64353933	0.03593148
Q5VW32	BRO1 domain-containing protein BROX	BROX	11.1	42.872	2.43025282	0.00954632
Q99816	Tumor susceptibility gene 101 protein	TSG101	15.9	40.917	2.40154634	0.00648237
O43657	Tetraspanin-6	TSPAN6	25.6	14.958	2.33242004	0.00169953
P05452	Tetranectin	CLEC3B	27.5	17.794	2.26469372	0.011433
P61313	Ribosomal protein L15	RPL15	15.2	19.338	2.25663371	0.00551006
P53990	IST1 homolog	IST1	57.3	23.375	2.25109795	0.00531066
P13010	X-ray repair cross-complementing protein 5	XRCC5	16.4	64.243	2.23381025	0.00371267
Q8J015	60S ribosomal protein L13a	RPL13A	14.3	23.558	2.13155137	0.02407208
Q9H9H4	Vacuolar protein sorting-associated protein 37B	VPS37B	9.2	20.654	2.09589466	0.02963136
P02461	Collagen alpha-1(III) chain	COL3A1	1.6	138.56	2.09300108	0.02280738
P27635	60S ribosomal protein L10	RPL10	40.7	12.285	2.08918466	0.03237894
Q8WUM4	Programmed cell death 6-interacting protein	PDCD6IP	39.6	96.022	2.05463106	0.00321507
P07237	Protein disulfide-isomerase	P4HB	14.2	16.215	2.04047326	0.0174391
Q9HD42	Charged multivesicular body protein 1a	CHMP1A	30.7	15.301	2.02701323	0.01108996

Table S2

Protein IDs	Protein names	Gene names	Sequence coverage [%]	Mol. weight [kDa]	SW620/ SW480	P. value
P11169	Solute carrier family 2, facilitated glucose transporter member 3	SLC2A3	20.8	31.874	0.011749168	0.0296785
O94832	Unconventional myosin-Id	MYO1D	28.2	116.2	0.038787995	0.00027188
P29374	Retinol-binding protein 1	RBP1	56	10.644	0.072787169	0.00388128
P98172	Ephrin-B1	EFNB1	16.2	38.006	0.074930021	0.00119442
P08133	Annexin A6	ANXA6	37.1	75.872	0.078012029	0.00031708
Q96TA1	Niban-like protein 1	C9orf88	10.9	82.682	0.126490412	0.01065253
Q9Y696	Chloride intracellular channel protein 4	CLIC4	26.6	26.694	0.137963444	0.03000887
P05556	Integrin beta-1	ITGB1	20.9	88.414	0.14864844	0.00146909
P16422	Epithelial cell adhesion molecule	EPCAM	34.8	37.893	0.163589346	0.00048008
P61081	NEDD8-conjugating enzyme Ubc12	UBE2M	8.7	20.9	0.165887295	0.0115204
P14222	Perforin-1	PRF1	29.7	61.346	0.166465764	0.00887923
Q969P0	Immunoglobulin superfamily member 8	IGSF8	21.2	65.033	0.168737967	1.6776E-05
O43707	Alpha-actinin-4	ACTN4	63.7	104.85	0.184502626	0.00046581
O00159	Unconventional myosin-Ic	MYO1C	21.8	118.99	0.196118715	0.00091981
O00468	Agrin	AGRN	27	203.09	0.204624716	0.00258642
P11166	Solute carrier family 2, facilitated glucose transporter member 1	SLC2A1	12.5	45.869	0.227212304	0.00028607
P10909	Clusterin	Clusterin	17.4	57.832	0.231262489	0.01649402
O75083	WD repeat-containing protein 1	WDR1	25.7	66.227	0.235138519	0.01728513
P18564	Integrin beta-6	ITGB6	1.3	75.849	0.238701666	0.00190898
P43007	Neutral amino acid transporter A	SLC1A4	2.4	47.726	0.248104871	0.00052163
Q01650	Large neutral amino acids transporter small subunit 1	SLC7A5	9.9	55.01	0.254952388	0.00514504
O00186	Syntaxin-binding protein 3	STXBP3	12	67.764	0.257123529	0.03321712
P63218	Guanine nucleotide-binding protein G(I)/G(S)/G(O) subunit gamma-5	GNG5	23.5	7.3184	0.258537813	0.01695074
P61026	Ras-related protein Rab-10	RAB10	20.5	22.541	0.260031307	0.0027144
P13987	CD59 glycoprotein	CD59	29.6	11.985	0.274520883	0.000113
Q15758	Neutral amino acid transporter B(0)	SLC1A5	25.9	56.583	0.275747651	7.5488E-05
Q9UHD8	Septin-9	Septin-9	22	23.971	0.279355157	0.00055609
P12814	Alpha-actinin-1	ACTN1	50.4	103.06	0.286041695	0.00051225
J3KPF3	4F2 cell-surface antigen heavy chain	SLC3A2	36.4	64.872	0.287544691	6.9295E-05
P55060	Exportin-2	CSE1L	5.6	110.42	0.29415306	0.01109174
P31947	14–3–3 protein sigma	SFN	43.1	27.774	0.294432959	0.00401826
Q16643	Drebrin	DBN1	14.8	36.471	0.320680503	0.02215882
P59998	Actin-related protein 2/3 complex subunit 4	ARPC4	19.9	21.058	0.324678693	0.00407438
P61006	Ras-related protein Rab-8A	RAB8A	25.1	23.668	0.324702465	0.03330491
V9HWH9	Protein S100-A11	S100A11	42.9	11.74	0.335125777	0.00294128
Q01518	Adenylyl cyclase-associated protein 1	CAP1	16.2	47.39	0.337232915	0.03235735
P48509	CD151 antigen	CD151	5.1	19.792	0.355641041	0.02287931
P17301	Integrin alpha-2	ITGA2	4.3	129.29	0.362271878	0.0435853
P26447	Protein S100-A4	S100A4	46.5	11.728	0.3624522	0.01947124
Q9H223	EH domain-containing protein 4	EHD4	35.1	61.155	0.370830425	0.00295808
Q1KLZ0	Actin, cytoplasmic 2	PS1TP5BP1	70.1	41.722	0.379410112	0.04247494
P27348	14–3–3 protein theta	YWHAQ	53.9	27.764	0.391324245	0.00384362
Q92522	Histone H1x	H1FX	26.3	22.487	0.394994486	0.02046652
P54709	Sodium/potassium-transporting ATPase subunit beta-3	ATP1B3	31.2	31.512	0.39581471	0.00900052
V9HWF5	Peptidyl-prolyl cis-trans isomerase A	PPIA	48.5	18.012	0.397199254	0.04077159
Q12959	Disks large homolog 1	DLG1	4.9	75.96	0.398631587	0.01565711
P62879	Guanine nucleotide-binding protein G(I)/G(S)/G(T) subunit beta-2	GNB2	48.5	37.331	0.402599067	0.00485033
P35241	Radixin	RDX	30	68.563	0.405935961	0.00974889
Q14847	LIM and SH3 domain protein 1	LASP1	26.4	29.645	0.406985226	0.01617477
P31431	Syndecan-4	SDC4	7.8	71.657	0.407307866	0.0159348
B6VEX4	Abl interactor 1	ABI1	9.3	42.637	0.407476812	0.02251877
Q9ULV4	Coronin-1C	CORO1C	21.9	53.28	0.40985014	0.00343122
Q86W92	Liprin-beta-1	PPFIBP1	7	114.02	0.41468217	0.02693422
P03971	Macrophage migration inhibitory factor	MIF	17.4	12.476	0.418381567	0.0001584
Q86VI3	Ras GTPase-activating-like protein IQGAP3	IQGAP3	4.5	179.48	0.420461641	0.02336381
P02786	Transferrin receptor protein 1	TFRC	21.7	84.872	0.425257535	0.00214362
P04439	HLA class I histocompatibility antigen, A alpha chain	HLA-A	34.8	31.623	0.427826788	0.01397475
P62136	Serine/threonine-protein phosphatase PP1-alpha catalytic subunit	PPP1CA	21.1	38.631	0.432666807	0.00477209
Q9NRW3	DNA dC->dU-editing enzyme APOBEC-3C	APOBEC3C	6.8	22.796	0.440265332	0.04194558
Q86 × 29	Lipolysis-stimulated lipoprotein receptor	LSR	23.4	64.346	0.440534774	0.00496959
P02649	Apolipoprotein E	APOE	27.1	36.154	0.440589659	0.01600696
P18085	ADP-ribosylation factor 4	ARF4	41.1	20.511	0.443431257	0.01993945
P55011	Solute carrier family 12 member 2	SLC12A2	8.8	129.72	0.443858211	0.00511427
P36873	Serine/threonine-protein phosphatase PP1-gamma catalytic subunit	PPP1CC	24.5	33.773	0.445747816	0.00223503
Q5ZPR3	CD276 antigen	CD276	10.3	41.709	0.447245301	0.00571664
V9HWB9	L-lactate dehydrogenase;L-lactate dehydrogenase A chain	LDHA	32.8	36.688	0.458180976	0.00041123
O15143	Actin-related protein 2/3 complex subunit 1B	ARPC1B	14.2	40.949	0.458231108	0.00228224
Q71UI9	Histone H2A.V	H2AFV	31.2	13.509	0.464114005	0.03317498
P21291	Cysteine and glycine-rich protein 1	CSRP1	33.8	16.94	0.468629793	0.02915667
V9HVZ4	Glyceraldehyde-3-phosphate dehydrogenase	GAPDH	46.9	36.053	0.46891796	0.00324459
Q8N5I2	Arrestin domain-containing protein 1	ARRDC1	9.2	29.254	0.470525512	0.0043285

(*continued on next page*)

(*continued*)

Protein IDs	Protein names	Gene names	Sequence coverage [%]	Mol. weight [kDa]	SW620/ SW480	P. value
P54707	Potassium-transporting ATPase alpha chain 2	ATP12A	4.6	115.51	0.474831724	0.00997908
P15529	Membrane cofactor protein	CD46	16.7	8.3916	0.476142784	0.00546069
Q9H5V8	CUB domain-containing protein 1	CDCP1	11.1	71.678	0.477411441	0.00845617
P05023	Sodium/potassium-transporting ATPase subunit alpha-1	ATP1A1	39.5	112.89	0.478365161	0.01275306
V9HWA6	Destrin	DSTN	46.7	18.506	0.484528666	0.03130172
P07355	Annexin A2	ANXA2	63.4	38.576	0.486185177	0.0028782
P46940	Ras GTPase-activating-like protein IQGAP1	IQGAP1	27.4	189.28	0.487387331	0.00379913
P63261	Actin-related protein 2/3 complex subunit 1B	ACTG1	70.1	41.792	0.489096205	0.0144896
O15144	Actin-related protein 2/3 complex subunit 2	ARPC2	9	34.333	0.492376837	0.01353878
P09327	Villin-1	VIL1	38.5	92.724	0.492763587	0.00680854
Q9H4M9	EH domain-containing protein 1	EHD1	21.3	60.626	0.492878223	0.00197344
P63000	Ras-related C3 botulinum toxin substrate 1	RAC1	40.6	21.45	0.496595902	0.00756952

Table S3

protein IDs	Protein names	Gene names	Sequence coverage [%]	Mol. weight [kDa]	Sequence coverage 480-mean [%]	Sequence coverage 620-mean [%]	Intensity	LFQ intensity 480-mean	LFQ intensity 620-mean
Q04941	Proteolipid protein 2	PLP2	8.6	16.691	0	5.733333	80,528,000	0	41,380,666.7
P31942	Heterogeneous nuclear ribonucleoprotein H3	HNRPH3	7.9	22.322	0	7.9	67,404,000	0	33,249,433.3
P15328	Folate receptor alpha	FOLR1	9.2	24.281	0	5.666667	37,123,000	0	19,172,000
Q05193	Dynamin-1	DNM1	12.2	35.248	0	8.133333	59,177,000	0	29,509,666.7
O00391	Sulfhydryl oxidase 1	QSOX1	4.1	66.821	2.2	1.333333	66,597,000	0	17,429,333.3
O00410	Importin-5	IPO5	4.2	81.23	0	2.8	24,252,000	0	12,211,666.7
Q96AY3	Peptidyl-prolyl cis-trans isomerase FKBP10	FKBP10	2.4	56.158	0	1.6	55,640,000	0	27,467,233.3
Q9UHB9	Signal recognition particle subunit SRP68	SRP68	4.2	60.226	0.833333	1.133333	14,730,000	0	7,536,333.33
Q13275	Semaphorin-3F	SEMA3F	7.2	30.259	0	4.8	39,158,000	0	19,862,666.7
P12830	Cadherin-1	CDH1	2.8	97.485	0.6	1	1.1E+08	0	49,516,333.3
P30408	Transmembrane 4 L6 family member 1	TM4SF1	8.9	10.989	0	8.9	50,396,000	0	25,707,000
P05067	Amyloid beta A4 protein	APP	8.5	54.981	0	5.033333	83,773,000	0	41,696,633.3
Q5HYI8	Rab-like protein 3	RABL3	20.8	5.5193	0	20.8	1.04E+08	0	50,064,666.7
P24821	Tenascin	TNC	34.3	220.85	12.43333	31.96667	8.61E+08	0	433,993,333
P63010	AP-2 complex subunit beta-1	AP2B1	7.3	18.606	0	4.866667	55,812,000	0	27,598,000
P26599	Polypyrimidine tract-binding protein 1	PTBP1	9	27.114	0	6	2.19E+08	0	108,196,667
P06241	Tyrosine-protein kinase Fyn	FYN	6.1	60.761	3.4	3.966667	40,373,000	0	20,373,000
P35326	Small proline-rich protein 2A	SPRR2A	43.1	7.9653	0	20.4	45,032,000	0	22,238,333.3
P25787	Proteasome subunit alpha type-2	PSMA2	13.2	25.84	1.433333	6	38,171,000	0	11,320,766.7
O00567	Nucleolar protein 56	NOP56	10.7	31.253	0	8.566667	36,208,000	0	18,588,333.3
Q5M9N0	Coiled-coil domain-containing protein 158	CCDC158	0.9	127.14	0.3	0.9	43,547,000	0	21,854,000
O94985	Calsyntenin-1	CLSTN1	2.7	88.039	0	2.033333	84,046,000	0	41,910,333.3
Q6P988	Palmitoleoyl-protein carboxylesterase NOTUM	NOTUM	4.8	55.699	0	3.8	73,588,000	0	37,186,666.7
P35232	Prohibitin	PHB	9.9	29.82	1.233333	4.133333	1.11E+08	0	55,058,533.3
O14986	Phosphatidylinositol 4-phosphate 5-kinase type-1 beta	STM7	4.5	37.786	0	4.5	3.03E+08	0	153,100,000
Q8NCR9	Clarin-3	CLRN3	12.4	25.321	3.866667	6.6	79,843,000	0	34,011,666.7
Q8NDC0	MAPK-interacting and spindle-stabilizing protein-like	MAPK1IP1L	6.9	24.269	0	4.6	58,364,000	0	30,015,333.3
Q8WUJ3	Cell migration-inducing and hyaluronan-binding protein	CEMIP	11.2	153	0	7.2	5.88E+08	0	283,110,000
Q92896	Golgi apparatus protein 1	GLG1	3.4	134.55	0	2.766667	1.37E+08	0	68,899,333.3
Q9H3U7	SPARC-related modular calcium-binding protein 2	SMOC2	17.7	49.674	0	16.86667	8.83E+08	0	448,096,667

Table S4

Protein IDs	Protein names	Gene names	Sequence coverage [%]	Mol. weight [kDa]	Sequence coverage 480-mean [%]	Sequence coverage 620-mean [%]	Intensity	LFQ intensity 480-mean	LFQ intensity 620-mean
P05121	Plasminogen activator inhibitor 1	SERPINE1	2.5	45.059	1.666666667	0	36,502,000	11,615,333.33	0
P50151	Guanine nucleotide-binding protein G(I)/G(S)/G(O) subunit gamma-10	GNG10	42.6	7.2053	42.6	0	98,311,000	29,713,666.67	0
P41221	Protein Wnt-5a	WNT5A	9	40.886	7	0	213,720,000	62,549,666.67	0
P31146	Coronin-1A	CORO1A	3.9	51.026	1.866666667	0	25,254,000	8,137,000	0
Q92817	Envoplakin	EVPL	0.4	231.63	0.4	0.133333333	22,870,000	6,611,900	0
P11234	Ras-related protein Ral-B	RALB	15.5	23.408	11.63333333	5.3	140,580,000	41,686,666.67	0
P14324	Farnesyl pyrophosphate synthase	FDPS	3.6	28.594	2.4	0	23,921,000	7,485,933.333	0
Q07157	Tight junction protein ZO-1	TJP1	1.4	187.85	1.166666667	0	84,367,000	24,778,666.67	0
P36969	Phospholipid hydroperoxide glutathione peroxidase	GPX4	10.4	15.438	6.933333333	0	12,080,000	3,787,700	0
P41250	Glycine–tRNA ligase	GARS	5	77.53	3.3	0	55,583,000	16,794,333.33	0
Q92598	Heat shock protein 105 kDa	HSPH1	6.1	88.841	4.1	0	72,896,000	21,843,000	0
P07954	Fumarate hydratase, mitochondrial	FH	7.5	54.636	4.5	0.966666667	70,255,000	16,694,400	0
P02792	Ferritin light chain	FTL	24.6	20.019	11.06666667	0	99,553,000	32,634,000	0
P23469	Receptor-type tyrosine-protein phosphatase epsilon	PTPRE	3.1	74.564	1.666666667	0	17,773,000	5,656,600	0
P50895	Basal cell adhesion molecule	BCAM	15.8	8.162	10.53333333	0	29,297,000	9,369,333.333	0
O43242	26S proteasome non-ATPase regulatory subunit 3	PSMD3	3	57.232	3	0	91,877,000	27,149,333.33	0
Q9NRY6	Phospholipid scramblase 3	PLSCR3	13.6	31.678	8.6	0.9	91,556,000	28,561,000	0
P43121	Cell surface glycoprotein MUC18	MCAM	7.7	59.019	5.966666667	0	339,680,000	100,331,333.3	0
P21980	Protein-glutamine gamma-glutamyltransferase 2	TGM2	18.8	68.648	17.56666667	0	1,175,800,000	351,616,666.7	0
P56199	Integrin alpha-1	ITGA1	3.2	130	2.033333333	0	142,870,000	42,286,666.67	0
P48059	LIM and senescent cell antigen-like-containing domain protein 1	LIMS1	23	13.705	14.8	0	47,810,000	13,719,666.67	0
B7Z2Q0	Actin filament-associated protein 1-like 2	AFAP1L2	3	97.193	3	0	112,520,000	33,462,666.67	0
B9EG73	Dedicator of cytokinesis protein 9	DOCK9	3.4	233.83	2.566666667	0	307,260,000	89,682,666.67	0
P09758	Tumor-associated calcium signal transducer 2	TACSTD2	16.7	35.723	15.46666667	0	90,281,000	26,570,666.67	0
P35080	Profilin-2	PFN2	15.4	9.7982	15.4	0	61,479,000	18,287,333.33	0
P99999	Cytochrome c	CYCS	18.8	11.333	12.53333333	0	39,851,000	12,847,533.33	0
Q9H0Z9	RNA-binding protein 38	RBM38	8.9	13.604	8.9	0	184,370,000	55,261,333.33	0
O75390	Citrate synthase	CS	24.2	7.3535	16.13333333	0	51,753,000	14,528,333.33	0
O95456	Proteasome assembly chaperone 1	PSMG1	15.9	7.182	10.6	0	20,264,000	6,455,133.333	0
P09496	Clathrin light chain A	CLTA	3.5	27.818	3.5	0	72,129,000	21,608,000	0
P60983	Glia maturation factor beta	GMFB	33.3	17.512	15.96666667	0	95,964,000	30,852,666.67	0
Q9Y4F1	FERM, RhoGEF and pleckstrin domain-containing protein 1	FARP1	6	24.749	4	0	23,814,000	6,839,166.667	0
P62714	Serine/threonine-protein phosphatase 2A catalytic subunit beta isoform	PPP2CB	16.9	13.87	11.26666667	0	36,508,000	10,631,333.33	0
Q13330	Metastasis-associated protein MTA1	MTA1	21.8	5.8987	21.8	0	31,412,000	9,423,566.667	0
O95471	Claudin-7	CLDN7	25.6	13.649	21.46666667	0	189,410,000	56,309,666.67	0
Q13433	Zinc transporter ZIP6	SLC39A6	4.4	30.912	2.933333333	0	46,342,000	14,534,333.33	0
Q08828	Adenylate cyclase type 1	ADCY1	12.5	8.7119	12.5	0	32,293,000	9,449,100	0
O15230	Laminin subunit alpha-5	LAMA5	2.4	399.73	1.9	0	228,260,000	68,682,666.67	0
O60635	Tetraspanin-1	TSPAN1	5.4	26.301	5.4	0	162,040,000	48,687,000	0
P09758	Tumor-associated calcium signal transducer 2	TACSTD2	16.7	35.709	15.46666667	0	264,340,000	77,985,333.33	0
P62760	Visinin-like protein 1	VSNL1	19.9	22.142	10.63333333	0	207,320,000	60,677,000	0
Q03405	Urokinase plasminogen activator surface receptor	PLAUR	30.1	36.978	21.8	0	421,970,000	126,686,666.7	0
O75874	Isocitrate dehydrogenase [NADP] cytoplasmic	IDH1	6.5	41.832	3.333333333	0	56,665,000	17,600,000	0
Q12846	Syntaxin-4	STX4	9.1	34.18	7.866666667	0	114,630,000	33,291,000	0
Q13200	26S proteasome non-ATPase regulatory subunit 2	PSMD2	2.5	64.587	2.5	0	21,373,000	6,739,400	0

(*continued on next page*)

(*continued*)

Protein IDs	Protein names	Gene names	Sequence coverage [%]	Mol. weight [kDa]	Sequence coverage 480-mean [%]	Sequence coverage 620-mean [%]	Intensity	LFQ intensity 480-mean	LFQ intensity 620-mean
P19256	Lymphocyte function-associated antigen 3	CD58	10.1	13.732	8.966666667	0	45,701,000	13,166,000	0
O00487	26S proteasome non-ATPase regulatory subunit 14	PSMD14	16.9	16.532	11.26666667	0	42,554,000	13,452,333.33	0
P36543	V-type proton ATPase subunit E 1	ATP6V1E1	5.8	26.145	3.866666667	0	13,687,000	3,852,366.667	0
Q54A15	Fermitin family homolog 1	FERMT1	9.9	77.408	6.633333333	0	170,830,000	50,556,666.67	0
Q562Z4	Actin-like protein	ACT	33	11.555	29.76666667	23.3	48,586,000	13,652,666.67	0
P08183	Multidrug resistance protein 1	ABCB1	3	116.72	2	0	82,775,000	24,464,700	0
O14936	Peripheral plasma membrane protein CASK	CASK	7.8	66.603	4.866666667	0	128,100,000	36,728,333.33	0
P05362	Intercellular adhesion molecule 1	ICAM1	11.3	57.768	11.3	0	292,830,000	87,657,666.67	0
Q14683	Structural maintenance of chromosomes protein 1A	SMC1A	6	48.887	3.266666667	1.366666667	95,721,000	23,194,000	0
Q6FHV6	Gamma-enolase	ENO2	15.2	47.268	11.5	7.5	36,401,000	11,354,700	0
P00492	Hypoxanthine-guanine phosphoribosyltransferase	HPRT1	16.1	24.588	9.033333333	0	49,736,000	14,969,666.67	0
P32004	Neural cell adhesion molecule L1	L1CAM	4.5	59.802	2.133333333	0	17,346,000	4,990,466.667	0
Q13509	Tubulin beta-3 chain	TUBB3	34	45.622	29.06666667	25.76666667	94,686,000	16,839,333.33	0
Q9UBT3	Dickkopf-related protein 4	DKK4	33.5	24.875	33.16666667	0	1,338,800,000	396,080,000	0
P30044	Peroxiredoxin-5	PRDX5	56.2	17.031	32.5	0	458,660,000	147,806,666.7	0

CRediT authorship contribution statement

Xinlu Liu: Methodology, Software, Validation, Formal analysis, Data curation, Writing – original draft, Writing – review & editing, Visualization, Supervision. **Na Li:** Software, Formal analysis, Data curation, Writing – original draft, Visualization. **Chi Zhang:** Formal analysis, Writing – original draft, Visualization. **Xiaoyu Wu:** Formal analysis, Writing – original draft. **Shoujia Zhang:** Writing – original draft. **Gang Dong:** Writing – original draft. **Ge Liu:** Methodology.

Declaration of Competing Interest

The authors declare no conflict of interest.

Acknowledgements

We acknowledge the technical support of this work by Shanghai Bioprofile Technology Company Ltd. We also acknowledge the financially supported in this work by Genetron Holdings Limited Corporation. We are also grateful for the English language editing from Editage (www.editage.cn).

References

[1] R.L. Siegel, K.D. Miller, H.E. Fuchs, A. Jemal, Cancer statistics, 2021, CA Cancer J. Clin. 71 (2021) 7–33.
[2] M.G. Fakih, Metastatic colorectal cancer: current state and future directions, J. Clin. Oncol. 33 (2015) 1809–1824.
[3] D. Basak, M.N. Uddin, J. Hancock, The role of oxidative stress and its counteractive utility in colorectal cancer (CRC), Cancers 12 (2020).
[4] K.G.K. Deepak, R. Vempati, G.P. Nagaraju, V.R. Dasari, N. S, D.N. Rao, R.R. Malla, Tumor microenvironment: challenges and opportunities in targeting metastasis of triple negative breast cancer, Pharmacol. Res. 153 (2020), 104683.
[5] K. Al-Nedawi, B. Meehan, J. Rak, Microvesicles: messengers and mediators of tumor progression, Cell Cycle 8 (2009) 2014–2018.
[6] H. Shao, H. Im, C.M. Castro, X. Breakefield, R. Weissleder, H. Lee, New technologies for analysis of extracellular vesicles, Chem. Rev. 118 (2018) 1917–1950.
[7] A.J. Guo, F.J. Wang, Q. Ji, H.W. Geng, X. Yan, L.Q. Wang, W.W. Tie, X.Y. Liu, R. F. Thorne, G. Liu, A.M. Xu, Proteome analyses reveal S100A11, S100P, and RBM25 are tumor biomarkers in colorectal cancer, Proteomics Clin. Appl. (2020), e2000056.
[8] P. Shannon, A. Markiel, O. Ozier, N.S. Baliga, J.T. Wang, D. Ramage, N. Amin, B. Schwikowski, T. Ideker, Cytoscape: a software environment for integrated models of biomolecular interaction networks, Genome Res. 13 (2003) 2498–2504.
[9] X. Liu, Y. Weng, P. Liu, Z. Sui, L. Zhou, Y. Huang, L. Zhang, Y. Zhang, X. Tan, Identification of PGAM1 as a putative therapeutic target for pancreatic ductal adenocarcinoma metastasis using quantitative proteomics, Onco Targets Ther. 11 (2018) 3345–3357.
[10] E. Tassi, R.T. Henke, E.T. Bowden, M.R. Swift, D.P. Kodack, A.H. Kuo, A. Maitra, A. Wellstein, Expression of a fibroblast growth factor-binding protein during the development of adenocarcinoma of the pancreas and colon, Cancer Res. 66 (2006) 1191–1198.
[11] T. Okamoto, Y. Tanaka, M. Kan, A. Sakamoto, K. Takada, J.D. Sato, Expression of fibroblast growth factor binding protein HBp17 in normal and tumor cells, *In Vitro* Cell. Dev. Biol. Anim. 32 (1996) 69–71.
[12] A. Aigner, H. Renneberg, J. Bojunga, J. Apel, P.S. Nelson, F. Czubayko, Ribozyme-targeting of a secreted FGF-binding protein (FGF-BP) inhibits proliferation of prostate cancer cells in vitro and in vivo, Oncogene 21 (2002) 5733–5742.
[13] B.L. Kagan, R.T. Henke, R. Cabal-Manzano, G.E. Stoica, Q. Nguyen, A. Wellstein, A. T. Riegel, Complex regulation of the fibroblast growth factor-binding protein in MDA- MB-468 breast cancer cells by CCAAT/enhancer-binding protein beta, Cancer Res. 63 (2003) 1696–1705.
[14] J. Chen, Q.M. Liu, P.C. Du, D. Ning, J. Mo, H.D. Zhu, C. Wang, Q.Y. Ge, Q. Cheng, X.W. Zhang, Y.W. Fan, H.F. Liang, L. Chu, X.P. Chen, B.X. Zhang, L. Jiang, Type-2 11beta-hydroxysteroid dehydrogenase promotes the metastasis of colorectal cancer via the Fgfbp1-AKT pathway, Am. J. Cancer Res. 10 (2020) 662–673.
[15] Z. Zhang, M. Liu, Q. Hu, W. Xu, W. Liu, Q. Sun, Z. Ye, G. Fan, X. Xu, X. Yu, S. Ji, Y. Qin, FGFBP1, a downstream target of the FBW7/c-Myc axis, promotes cell proliferation and migration in pancreatic cancer, Am. J. Cancer Res. 9 (2019) 2650–2664.
[16] O.M. Tsygankova, C. Ma, W. Tang, C. Korch, M.D. Feldman, Y. Lv, M.S. Brose, J. L. Meinkoth, Downregulation of Rap1GAP in human tumor cells alters cell/matrix and cell/cell adhesion, Mol. Cell. Biol. 30 (2010) 3262–3274.
[17] K. Kometani, D. Ishida, M. Hattori, N. Minato, Rap1 and SPA-1 in hematologic malignancy, Trends Mol. Med. 10 (2004) 401–408.
[18] M. Hattori, N. Minato, Rap1 GTPase: functions, regulation, and malignancy, J. Biochem. 134 (2003) 479–484.
[19] Y. Shimizu, Y. Hamazaki, M. Hattori, K. Doi, N. Terada, T. Kobayashi, Y. Toda, T. Yamasaki, T. Inoue, Y. Kajita, A. Maeno, T. Kamba, Y. Mikami, T. Kamoto, T. Yamada, T. Kanno, K. Yoshikawa, O. Ogawa, N. Minato, E. Nakamura, SPA-1 controls the invasion and metastasis of human prostate cancer, Cancer Sci. 102 (2011) 828–836.
[20] J. Kodama, I. Hashimoto, N. Seki, A. Hongo, M. Yoshinouchi, H. Okuda, T. Kudo, Thrombospondin-1 and -2 messenger RNA expression in invasive cervical cancer: correlation with angiogenesis and prognosis, Clin. Cancer Res. 7 (2001) 2826–2831.
[21] M. Yamaguchi, K. Sugio, K. Ondo, T. Yano, K. Sugimachi, Reduced expression of thrombospondin-1 correlates with a poor prognosis in patients with non-small cell lung cancer, Lung Cancer 36 (2002) 143–150.
[22] E. Ioachim, K. Damala, E. Tsanou, E. Briasoulis, E. Papadiotis, A. Mitselou, A. Charhanti, M. Doukas, L. Lampri, D.L. Arvanitis, Thrombospondin-1 expression

in breast cancer: prognostic significance and association with p53 alterations, tumour angiogenesis and extracellular matrix components, Histol. Histopathol. 27 (2012) 209–216.
[23] H. Teraoku, Y. Morine, T. Ikemoto, Y. Saito, S. Yamada, M. Yoshikawa, C. Takasu, J. Higashijima, S. Imura, M. Shimada, Role of thrombospondin-1 expression in colorectal liver metastasis and its molecular mechanism, J. Hepatobiliary Pancreat. Sci. 23 (2016) 565–573.
[24] B. Chiavarina, B. Costanza, R. Ronca, A. Blomme, S. Rezzola, P. Chiodelli, A. Giguelay, G. Belthier, G. Doumont, G. Van Simaeys, S. Lacroix, T. Yokobori, B. Erkhem-Ochir, P. Balaguer, V. Cavailles, E. Fabbrizio, E. Di Valentin, S. Gofflot, O. Detry, G. Jerusalem, S. Goldman, P. Delvenne, A. Bellahcene, J. Pannequin, V. Castronovo, A. Turtoi, Metastatic colorectal cancer cells maintain the TGFbeta program and use TGFBI to fuel angiogenesis, Theranostics 11 (2021) 1626–1640.
[25] Z. Li, R.T. Luo, S. Mi, M. Sun, P. Chen, J. Bao, M.B. Neilly, N. Jayathilaka, D. S. Johnson, L. Wang, C. Lavau, Y. Zhang, C. Tseng, X. Zhang, J. Wang, J. Yu, H. Yang, S.M. Wang, J.D. Rowley, J. Chen, M.J. Thirman, Consistent deregulation of gene expression between human and murine MLL rearrangement leukemias, Cancer Res. 69 (2009) 1109–1116.
[26] S. Kang, S.M. Dong, N.H. Park, Frequent promoter hypermethylation of TGFBI in epithelial ovarian cancer, Gynecol. Oncol. 118 (2010) 58–63.
[27] J.N. Shah, G. Shao, T.K. Hei, Y. Zhao, Methylation screening of the TGFBI promoter in human lung and prostate cancer by methylation-specific PCR, BMC Cancer 8 (2008) 284.
[28] H. Tomioka, K. Morita, S. Hasegawa, K. Omura, Gene expression analysis by cDNA microarray in oral squamous cell carcinoma, J. Oral Pathol. Med. 35 (2006) 206–211.
[29] K.G. Owusu-Ansah, G. Song, R. Chen, M.I.A. Edoo, J. Li, B. Chen, J. Wu, L. Zhou, H. Xie, D. Jiang, S. Zheng, COL6A1 promotes metastasis and predicts poor prognosis in patients with pancreatic cancer, Int. J. Oncol. 55 (2019) 391–404.
[30] T. Hou, C. Tong, G. Kazobinka, W. Zhang, X. Huang, Y. Huang, Y. Zhang, Expression of COL6A1 predicts prognosis in cervical cancer patients, Am. J. Transl. Res. 8 (2016) 2838–2844.
[31] K.H. Chiu, Y.H. Chang, Y.S. Wu, S.H. Lee, P.C. Liao, Quantitative secretome analysis reveals that COL6A1 is a metastasis-associated protein using stacking gel-aided purification combined with iTRAQ labeling, J. Proteome Res. 10 (2011) 1110–1125.
[32] Z. Jian, T. Cheng, Z. Zhang, S. Raulefs, K. Shi, K. Steiger, N. Maeritz, K. Kleigrewe, T. Hofmann, S. Benitz, P. Bruns, D. Lamp, M. Jastroch, J. Akkan, C. Jager, P. Huang, S. Nie, S. Shen, X. Zou, G.O. Ceyhan, C.W. Michalski, H. Friess, J. Kleeff, B. Kong, Glycemic Variability Promotes Both Local Invasion and Metastatic Colonization by Pancreatic Ductal Adenocarcinoma, Cell Mol. Gastroenterol. Hepatol. 6 (2018) 429–449.
[33] Y.H. Nguyen, A.A. Mills, E.J. Stanbridge, Assembly of the QM protein onto the 60S ribosomal subunit occurs in the cytoplasm, J. Cell. Biochem. 68 (1998) 281–285.
[34] J. Shi, L. Zhang, D. Zhou, J. Zhang, Q. Lin, W. Guan, J. Zhang, W. Ren, G. Xu, Biological Function of Ribosomal Protein L10 on Cell Behavior in Human Epithelial Ovarian Cancer, J. Cancer 9 (2018) 745–756.
[35] S. Aras, M.R. Zaidi, TAMeless traitors: macrophages in cancer progression and metastasis, Br. J. Cancer 117 (2017) 1583–1591.
[36] G. Altinok, I.J. Powell, M. Che, K. Hormont, F.H. Sarkar, W.A. Sakr, D. Grignon, D. J. Liao, Reduction of QM protein expression correlates with tumor grade in prostatic adenocarcinoma, Prostate Cancer Prostatic Dis. 9 (2006) 77–82.
[37] T. Girardi, S. Vereecke, S.O. Sulima, Y. Khan, L. Fancello, J.W. Briggs, C. Schwab, J. O. de Beeck, J. Verbeeck, J. Royaert, E. Geerdens, C. Vicente, S. Bornschein, C. J. Harrison, J.P. Meijerink, J. Cools, J.D. Dinman, K.R. Kampen, K. De Keersmaecker, The T-cell leukemia-associated ribosomal RPL10 R98S mutation enhances JAK-STAT signaling, Leukemia 32 (2018) 809–819.
[38] F. Graziano, A. Ruzzo, E. Giacomini, T. Ricciardi, G. Aprile, F. Loupakis, P. Lorenzini, E. Ongaro, F. Zoratto, V. Catalano, D. Sarti, E. Rulli, C. Cremolini, M. De Nictolis, G. De Maglio, A. Falcone, G. Fiorentini, M. Magnani, Glycolysis gene expression analysis and selective metabolic advantage in the clinical progression of colorectal cancer, Pharmacogenomics J. 17 (2017) 258–264.
[39] E. Kim, S. Jung, W.S. Park, J.H. Lee, R. Shin, S.C. Heo, E.K. Choe, J.H. Lee, K. Kim, Y.J. Chai, Upregulation of SLC2A3 gene and prognosis in colorectal carcinoma: analysis of TCGA data, BMC Cancer 19 (2019) 302.
[40] X. Yao, Z. He, C. Qin, X. Deng, L. Bai, G. Li, J. Shi, SLC2A3 promotes macrophage infiltration by glycolysis reprogramming in gastric cancer, Cancer Cell Int. 20 (2020) 503.
[41] J.L. Napoli, Cellular retinoid binding-proteins, CRBP, CRABP, FABP5: effects on retinoid metabolism, function and related diseases, Pharmacol. Ther. 173 (2017) 19–33.
[42] J.A. Silvaroli, J.M. Arne, S. Chelstowska, P.D. Kiser, S. Banerjee, M. Golczak, Ligand binding induces conformational changes in human cellular retinol-binding protein 1 (CRBP1) revealed by atomic resolution crystal structures, J. Biol. Chem. 291 (2016) 8528–8540.
[43] V. Dobrotkova, P. Chlapek, P. Mazanek, J. Sterba, R. Veselska, Traffic lights for retinoids in oncology: molecular markers of retinoid resistance and sensitivity and their use in the management of cancer differentiation therapy, BMC Cancer 18 (2018) 1059.
[44] J.A. Silvaroli, M.A.K. Widjaja-Adhi, T. Trischman, S. Chelstowska, S. Horwitz, S. Banerjee, P.D. Kiser, W.S. Blaner, M. Golczak, Abnormal Cannabidiol Modulates Vitamin A Metabolism by Acting as a Competitive Inhibitor of CRBP1, ACS Chem. Biol. 14 (2019) 434–448.
[45] A.P. Chou, R. Chowdhury, S. Li, W. Chen, A.J. Kim, D.E. Piccioni, J.M. Selfridge, R. R. Mody, S. Chang, S. Lalezari, J. Lin, D.E. Sanchez, R.W. Wilson, M.C. Garrett, B. Harry, J. Mottahedeh, P.L. Nghiemphu, H.I. Kornblum, P.S. Mischel, R.M. Prins, W.H. Yong, T. Cloughesy, S.F. Nelson, L.M. Liau, A. Lai, Identification of retinol binding protein 1 promoter hypermethylation in isocitrate dehydrogenase 1 and 2 mutant gliomas, J. Natl. Cancer Inst. 104 (2012) 1458–1469.
[46] K. Toki, H. Enokida, K. Kawakami, T. Chiyomaru, S. Tatarano, H. Yoshino, Y. Uchida, K. Kawahara, K. Nishiyama, N. Seki, M. Nakagawa, CpG hypermethylation of cellular retinol-binding protein 1 contributes to cell proliferation and migration in bladder cancer, Int. J. Oncol. 37 (2010) 1379–1388.
[47] R. Peralta, A. Valdivia, I. Alvarado-Cabrero, F. Gallegos, T. Apresa, D. Hernandez, M. Mendoza, P. Romero, L. Paniagua, M. Ibanez, L. Cabrera, M. Salcedo, Correlation between expression of cellular retinol-binding protein 1 and its methylation status in larynx cancer, J. Clin. Pathol. 65 (2012) 46–50.
[48] L. Gao, Q. Wang, W. Ren, J. Zheng, S. Li, Z. Dou, X. Kong, X. Liang, K. Zhi, The RBP1-CKAP4 axis activates oncogenic autophagy and promotes cancer progression in oral squamous cell carcinoma, Cell Death. Dis. 11 (2020) 488.
[49] A. Shvab, G. Haase, A. Ben-Shmuel, N. Gavert, T. Brabletz, S. Dedhar, A. Ben-Ze'ev, Induction of the intestinal stem cell signature gene SMOC-2 is required for L1-mediated colon cancer progression, Oncogene 35 (2016) 549–557.
[50] P. Liu, J. Lu, W.V. Cardoso, C. Vaziri, The SPARC-related factor SMOC-2 promotes growth factor-induced cyclin D1 expression and DNA synthesis via integrin-linked kinase, Mol. Biol. Cell 19 (2008) 248–261.
[51] J.R. Su, J.H. Kuai, Y.Q. Li, Smoc2 potentiates proliferation of hepatocellular carcinoma cells via promotion of cell cycle progression, World J. Gastroenterol. 22 (2016) 10053–10063.
[52] J.J. Brady, C.H. Chuang, P.G. Greenside, Z.N. Rogers, C.W. Murray, D.R. Caswell, U. Hartmann, A.J. Connolly, E.A. Sweet-Cordero, A. Kundaje, M.M. Winslow, An Arntl2-driven secretome enables lung adenocarcinoma metastatic self-sufficiency, Cancer Cell 29 (2016) 697–710.
[53] B.G. Jang, H.S. Kim, J.M. Bae, W.H. Kim, H.U. Kim, G.H. Kang, SMOC2, an intestinal stem cell marker, is an independent prognostic marker associated with better survival in colorectal cancers, Sci. Rep. 10 (2020) 14591.
[54] M. Esposito, N. Mondal, T.M. Greco, Y. Wei, C. Spadazzi, S.C. Lin, H. Zheng, C. Cheung, J.L. Magnani, S.H. Lin, I.M. Cristea, R. Sackstein, Y. Kang, Bone vascular niche E-selectin induces mesenchymal-epithelial transition and Wnt activation in cancer cells to promote bone metastasis, Nat. Cell Biol. 21 (2019) 627–639.
[55] T. Morisaki, M. Yashiro, A. Kakehashi, A. Inagaki, H. Kinoshita, T. Fukuoka, H. Kasashima, G. Masuda, K. Sakurai, N. Kubo, K. Muguruma, M. Ohira, H. Wanibuchi, K. Hirakawa, Comparative proteomics analysis of gastric cancer stem cells, PLoS One 9 (2014), e110736.
[56] C. Kuscu, N. Evensen, D. Kim, Y.J. Hu, S. Zucker, J. Cao, Transcriptional and epigenetic regulation of KIAA1199 gene expression in human breast cancer, PLoS One 7 (2012) e44661.
[57] M. Terashima, Y. Fujita, Y. Togashi, K. Sakai, M.A. De Velasco, S. Tomida, K. Nishio, KIAA1199 interacts with glycogen phosphorylase kinase beta-subunit (PHKB) to promote glycogen breakdown and cancer cell survival, Oncotarget 5 (2014) 7040–7050.
[58] J. Sabates-Bellver, L.G. Van der Flier, M. de Palo, E. Cattaneo, C. Maake, H. Rehrauer, E. Laczko, M.A. Kurowski, J.M. Bujnicki, M. Menigatti, J. Luz, T. V. Ranalli, V. Gomes, A. Pastorelli, R. Faggiani, M. Anti, J. Jiricny, H. Clevers, G. Marra, Transcriptome profile of human colorectal adenomas, Mol. Cancer Res. 5 (2007) 1263–1275.
[59] L.C. LaPointe, S.K. Pedersen, R. Dunne, G.S. Brown, L. Pimlott, S. Gaur, A. McEvoy, M. Thomas, D. Wattchow, P.L. Molloy, G.P. Young, Discovery and validation of molecular biomarkers for colorectal adenomas and cancer with application to blood testing, PLoS One 7 (2012) e29059.